Local environmental context drives heterogeneity of early succession dynamics in alpine glacier forefields

Arthur Bayle[1†*], Bradley Z. Carlson[2†], Anaïs Zimmer[3], Sophie Vallée[4], Antoine Rabatel[5], Edoardo Cremonese[6], Gianluca Filippa[6], Cédric Dentant[7], Christophe Randin[8], Andrea Mainetti[9], Erwan Roussel[10], Simon Gascoin[11], Dov Corenblit[10] & Philippe Choler[1]

1Univ. Grenoble Alpes, Univ. Savoie Mont Blanc, CNRS, LECA, F-38000 Grenoble, France

2Centre de Recherches sur les Écosystèmes d'Altitude (CREA), Observatoire du Mont-Blanc, F-74400 Chamonix, France

3Department of Geography and the Environment, The University of Texas at Austin, Austin, Texas, USA

4Conservatoire Botanique National Alpin (CBNA), F-73000 Chambéry, France

5Univ. Grenoble Alpes, CNRS, IRD, Grenoble-INP, Institut des Géosciences de l'Environnement (IGE, UMR 5001), F-38000 Grenoble, France

6Environmental Protection Agency of Aosta Valley, Climate Change Unit, Loc. La Maladière, 48, IT-11020 Saint Christophe (AO), Italy

7Parc National des Ecrins, Domaine de Charance, Gap, France

8Univ. Lausanne, Dept. of Ecology & Evolution / Interdisciplinary Centre for Mountain Research (CIRM), Biophore, CH-1015 Lausanne, Switzerland

9Biodiversity Service and Scientific Research, Gran Paradiso National Park, Torino, Italy

10Université Clermont Auvergne, CNRS, GEOLAB, Clermont-Ferrand, France

11CESBIO, Université de Toulouse, CNES/CNRS/IRD/INRAE/UPS, Toulouse, France

†These authors contributed equally to this work

Correspondence to: Arthur Bayle (arthur.bayle.env@gmail.com)

Abstract. Glacier forefields have long provided ecologists with a model to study patterns of plant succession following glacier retreat. While plant survey-based approaches applied along chronosequences provide invaluable information on plant communities, the "space-for-time" approach assumes environmental uniformity and equal ecological potential across sites and does not account for spatial variability in initial site conditions. Remote sensing provides a promising avenue for assessing plant colonisation dynamics using a so-called "real-time" approach. Here, we combined 36 years of Landsat imagery with extensive field sampling along chronosequences of deglaciation for eight glacier forefields in the south-western European Alps to investigate the heterogeneity of early plant succession dynamics. Based on the two complementary and independent approaches, we found strong variability in the time lag between deglaciation and colonisation by plants and in subsequent growth rates, and in the composition of early plant succession. All three parameters were highly dependent on the local environmental context, i.e., neighbouring vegetation cover and energy availability linked to temperature and snowmelt gradients. Potential geomorphological disturbance did not emerge as a strong predictor of succession parameters, perhaps due to insufficient spatial resolution of predictor variables. Notably, the identity of pioneer plant species was highly variable, and initial plant community composition had a much stronger influence on plant assemblages than elapsed time since deglaciation. Overall, both approaches converged towards the conclusion that early plant succession is not stochastic as previous authors have suggested but rather determined by local ecological context. We discuss the importance of scale in deciphering the complexity of plant succession in glacier forefields and provide recommendations for improving botanical field surveys and using Landsat time series in glacier forefields systems. Our work demonstrates complementarity between remote sensing and field-based approaches for both understanding and predicting future patterns of plant succession in glacier forefields.

1 Introduction

Glaciers in the European Alps began to retreat around the mid-19th century in response to changes in climate conditions driven first by shifts in precipitation (Vincent et al., 2005) and then by human-induced changes in aerosol concentrations in the atmosphere combined with warming (Painter et al., 2013, Sigl et al., 2018). Pronounced glacier retreat marked the end of the Little Ice Age (LIA), a multi-century period during which glacier terminal moraines were up to a few kilometers down valley from their current location (Matthews and Briffa, 2005, Gardent et al., 2014). As glaciers retreat, the surface area of the glacier forefields (i.e., the area extending between the glacier snout and the moraine deposited during the LIA maximum extent) increases (Marta et al., 2021). Over the 20th century, the pace of glacier retreat in the Alps was variable and punctuated by a few brief glacier advances. However, this variability has given way to consistent and accelerating melting since the 1990s (Vincent et al., 2014), in response to warming air temperatures and associated reductions in snowpack depth and duration (Gobiet et al., 2014). In this context, recently deglaciated areas constitute particularly dynamic ecosystems that are reshaping high mountain landscapes (Haeberli et al., 2017) and associated biodiversity and ecosystem services (Cauvy-Fraunie and Dangles, 2019, Ficetola et al., 2021). These emerging ecosystems have been identified as hotspots of the widespread greening observed throughout the European Alps during recent decades (Bayle, 2020, Choler et al., 2021, Carlson et al., 2017; Dentant et al. 2022), calling for the need to better understand plant colonization dynamics in glacier forefields to predict future trajectories of alpine ecosystems (Huss et al., 2017).

Glacier forefields have long provided ecologists with a model to study patterns of plant succession along chronosequences of glacier retreat (Chapin et al., 1994), most often using a "space-for-time" approach (Pickett, 1989, Zimmer et al., 2018). This method relies on the assumption that within a glacier forefield, initial environmental conditions are consistent, and that pioneer species benefit from equal opportunity for establishment and growth over space and time (Johnson and Miyanishi, 2008). However, field observations accompanied by a growing body of literature indicate that this approach is overly simplistic given the environmental heterogeneity of glacier forefields as well as the complexity of biological processes involved. Indeed, we now know that plant succession rates and trajectories are controlled by both abiotic and biotic processes, which in turn depend on regional landscape and local environmental factors, such as micro-climate (Joly and Brossard, 2007), substrate and disturbance regimes (Anthelme et al., 2021, Eichel et al., 2016), water and nutrient availability (Górniak et al., 2017), micro-topography (Raffl et al., 2006, Scherrer and Körner, 2011) and broad scale gradients such as elevation and continentality (Garibotti et al., 2011, Rydgren et al., 2014, Robbins and Matthews, 2010, Robbins and Matthews, 2014). All these factors can lead to strong heterogeneity in vegetation dynamics within and between glacier forefields.

Plant succession dynamics in glacier forefields, as elsewhere, can be broken down into three fundamental steps (Bradshaw, 1993): (i) diaspores reaching areas of bare ground, i.e., dispersal, (ii) successful and persistent establishment, and (iii) plant succession, as community composition matures and develops over time. Wojcik et al. (2021) recently proposed a novel conceptual model aimed at better understanding and predicting contrasting trajectories of plant succession dynamics in glacier forefields based on the complex interplay between autogenic factors, i.e., time dependent biological succession, and allogenic factors, i.e., external environmental factors such as climate or geomorphological disturbances. The authors suggest that the importance of autogenic and allogenic components varies over time, with an initial stochastic phase (i.e., dispersal) followed by a more deterministic phase defined by environmental factors, biological interactions, and bio geomorphic feedbacks (Eichel et al., 2016). Contrasting succession trajectories within glacier forefields are presented as the result of variations in (i) time since glacier retreat; (ii) initial site conditions (heterogeneous micro-climate, substrate properties and resource availability); and (iii) geomorphological disturbances (hillslope, torrential, periglacial, aeolian disturbances). In addition to time, autogenic biological properties also shape plant succession dynamics: regional species pool composition determines propagule pressure,

2

while plant functional traits (wind dispersal and low seed mass) facilitate the arrival and establishment of pioneer species (Franzén et al., 2019, Rosero et al., 2021, Schumann et al., 2016). At broader scales, variability in plant succession rates between glacier forefields has been linked to elevation and continentality, which in turn influence more direct environmental parameters such as temperature and snow cover duration (Robbins and Matthews, 2010).

In addition to assuming environmental uniformity and equal ecological potential over space, plant survey-based approaches applied along chronosequences yield only a snapshot of plant community properties and fail to provide insights into the temporal dynamics of succession. To address questions linking auto- and allogenic factors to time lags, i.e., time between a surface deglaciation and its initial plant establishment, it appears necessary to adopt a "real-time" approach based on annually resolved information on plant succession dynamics. While some studies have successfully implemented repeat surveys of permanent plots in the context of glacier forefields (Fickert and Grüninger, 2018) repeat field surveys of plant communities in often remote and hard-to-access mountain environments present major challenges in terms of cost and effort.

As a complementary approach to traditional plot-based surveys, which remain essential to understand   biogeomorphic processes on the ground, remote sensing provides a promising avenue for assessing plant colonization dynamics within and between glacier forefields using a so-called "real-time" approach. Beginning in 1984 with the Landsat 5 TM, followed by Landsat 7 ETM+ and Landsat 8 OLI sensors, Landsat satellites currently provide a 36-year archive of 30 m resolution images acquired at 16-day intervals over the globe's terrestrial areas. Availability of Landsat imagery since the mid-1980s allows for investigating plant succession dynamics since the most recent observed advance of alpine glaciers and in response to accelerating glacier retreat during recent decades. Vegetation indices such as the Normalized Difference Vegetation Index (NDVI) provide a proxy of plant biomass (Tucker and Sellers, 1986), photosynthetic activity and vegetation cover and have the potential to reliably quantify plant succession in rocky areas with low plant cover. As NDVI is a non-physical and uni-dimensional quantity based on remotely measured reflectance, variations in quantities over time can be disconnected from changes in plant cover on the ground, particularly in the context of heterogeneous topography (Bayle et al., 2021). In addition to systematic errors caused by sensor limitations, variation in NDVI over time can be due to atmospheric and cloud contamination (Masek et al., 2006), angular effects due to variation in sun-surface-sensor geometry or topography (Nagol et al., 2015, Martín-Ortega et al., 2020), sensor degradation and calibration changes (Markham and Helder, 2012) or between sensor spectral band pass (Steven et al., 2003). Overall, it has been shown that NDVI increases near-linearly with fractional vegetation cover (horizontal density) until values reach between 80% and 90% at which point it tends to saturate and increases slowly with increasing Leaf Area Index (vertical density). Remote sensing approaches have already been used efficiently in the context of glacier forefields (Klaar et al., 2015, Fischer et al., 2019, Bayle, 2020, Knoflach et al., 2021) and high sensitivity of Landsat-based NDVI to low plant cover has been demonstrated in glacier forefields (Bayle et al., 2021) and in Antarctica (Fretwell et al., 2011).

Here, we investigated early plant succession dynamics (0-35 years since glacier retreat) in the context of eight glaciers distributed across the southwestern European Alps. Specifically, we sought to answer the following ecological questions: (1) Is observed heterogeneity in early plant succession dynamics (time between deglaciation and plant colonisation, and plant growth rate following colonization) indeed purely stochastic or can this variability be linked to environmental factors? (2) Is early plant community composition consistent across sites and shaped by time availability or heterogeneous and driven by local environmental context ? To address these questions, we utilized two independent data sources: 36 years of Landsat imagery and 297 floristic field plots. First, we derived two indicators of vegetation dynamics from Landsat time series, which are (i) time lag between ice melting and detection of plant colonisation, and (ii) plant growth rate following colonization. Then, we investigated the spatial heterogeneity of these indicators and their respective drivers using proxies of the local environmental and geomorphological context (allogenic factors). Second, we assessed turnover in plant community composition between

and within the eight glacier forefields using a "space-for-time" approach and with regard to local environmental and geomorphological context (allogenic factors) and time since deglaciation (autogenic factor). Finally, we questioned the capacity of field sampling to capture heterogeneity in vegetation dynamics with respect to spatially exhaustive remote sensing approach, and we provide some recommendations to improve field sampling methodology for future studies. In addition to testing theoretical expectations in glacier forefields across a broad spectrum of environmental and ecological contexts, our study provides for the first time a clear roadmap for applying widely available remote sensing data to quantify and improve our understanding of trajectories of plant colonization and succession in glacier forefields.

2 Data and study site

2.1 Study site

Our study investigates eight glacier forefields distributed throughout the southwestern European Alps (Figure 1) in France (Glacier Blanc, Saint-Sorlin, Gébroulaz, Tour and Pélerins), Switzerland (Orny) and Italy (Lavassey and Lauson). Sites are distributed from 45° to 46° N and from 6° to 7° E across a variety of slopes and aspects, and elevations. Substrates are highly variable both within and between forefields including exposed bedrock, chaotic blocks of various sizes, gravel, and sand. Stream networks are often intricate, with strong seasonal and daily variability.

2.2 Age of deglaciation

Chronosequences of glacier outlines for the eight glaciers were initially obtained from various sources depending on the country. For France (GB, GEB, STS, PEL, TR), glacier outlines were extracted from the GLIMS database (Gardent et al. 2014) which contain outlines dating from 1985/86 based on Landsat 5 TM (30m), 2003 based on Landsat 5 TM and 7 ETM+ (30m), 2006, 2008 or 2009 (depending on the glacier) based on sub-meter resolution images from BD ORTHO IGN and finally 2014, 2016, 2018 (depending on the glacier) Spot 6/7 images (1.5 m). For Italy (LAU, LAV), glacier outlines for 1975 were obtained based on photo interpretation of Regional Technical Maps, 1999, 2005, 2012 and 2019 based on orthophoto (50 cm) and Sentinel-2 (10 m). For Switzerland (OR), glacier outlines were extracted from the GLAMOS database (Linsbauer et al., 2021). Overall, we were able to obtain chronosequences for the eight glaciers that approximately corresponded to the Landsat time series historical depth. As our glacier contours database mixed automatic and manual methods with sources at medium to high resolution, important quality differences were observed within and between glacier chronosequence as older contours were mostly based on coarse resolution images through automatic approaches that tend to perform poorly for debris-covered glaciers. To improve the consistency of our database and the reliability of further analysis, we carried out manual photo interpretation of sub-meter historical images for all glacier contours. For STS, TR, OR and LAV, small corrections were applied due only to the improvement of sources resolution, while for GEB, PEL and LAU, which are totally or partly covered by debris, we substantially improved the delimitation by accounting for emissary streams, crevasses and lateral screes reoriented by glacier movement. For GB, we also identified a large section of dead-ice that detached from the main glacier in 2014, and which remains in 2021 (Bayle, 2020). We removed this area from further analysis. Image sources are presented in Table S2 while detailed procedures to obtain our sub-meter glacier contours database are presented for each glacier in Figures S1 to S6. Glacier outlines were manually delineated using ArcGIS software (Esri, 10.4.1). A detailed description of the sources used to improve the glacier outlines dataset can be found in Table S1.

We estimated continuous years of deglaciation (YOD) from glacier outlines using an interpolation method initially designed for the creation of hydrologically corrected digital elevation models (DEMs). We used the Topo-to-raster function in ArcGIS based on the

149　ANUDEM program (Hutchinson et al., 2011), which is specifically designed to work with line features as input, to obtain a raster indicating

150　the YOD. Linear interpolation assumes that glaciers retreated at a constant rate between two dated glacier extents. To evaluate this

151　assumption, interpolated surfaces from Glacier Blanc were compared to a denser chronosequence of deglaciation from Bayle (2020) that

152　were not used in this work. The linear model between the results from interpolation and ground-truth observation obtained a R^2 of 0.945

153　with a mean error of +/- 2 years (Figure S7).

154

155　*2.3 Vegetation field surveys*

156　　　Glacier forefields of GB, GEB, STS, PEL, TR, LAV, LAU and OR were surveyed in the months of July and August in 2019 and

157　2020. For each forefield and chronosequence band (for example the zone deglaciated between 1983 to 2003), we generated a set of 15

158　random sampling points, while ensuring a minimum distance of five meters between sampling points. In the field we went as close as possible

159　to these points using a GPS and excluded sites that were too dangerous to access walking or that were under water or snow. For each plot,

160　within a 2x2m quadrat we surveyed the percent cover of vascular plants, mosses and lichens, biological soil crust (Khedim et al., 2021,

161　Breen and Lévesque, 2008), and bare ground (which was further subdivided into percent bedrock, sand, gravel < 2 cm, rocks between 2 and

162　20 cm and blocks larger than 20 cm in diameter). We also recorded all vascular plant species as well as their relative cover and average

163　vegetative height within the quadrat. We had a total of 297 plots with 59, 37, 36, 38, 27, 20, 28 and 52 plots for GB, GEB, LAU, LAV, OR,

164　PEL, STS and TR respectively.

165

166　*2.4 Remote sensing data*

167　　　Landsat 5 TM, Landsat 7 ETM+ and Landsat 8 OLI standard level 1 Terrain-corrected (L1T) orthorectified images from Collection

168　1 (geolocation error < 12 m) between 1984 and 2019 for 4 path/row (tiles) were downloaded from the Landsat Earth Explorer data portal

169　(http://earthexplorer.usgs.gov) at surface reflectance level of correction. Images with average cloud cover < 80% only were selected as high

170　cloud cover can reduce the number of available ground control points and therefore the geolocation accuracy, and because cloud masking

171　relies on clear-sky pixels to identify clouds. As a result, a total of 2846 scenes were selected, 60% of which were from Landsat 5. To improve

172　the robustness of our remote sensing analysis, we applied state of the art methods to correct for inter-sensor spectral variation, Bidirectional

173　Reflectance Distribution Function (BRDF) and illumination related errors, and to mask cloud and cloud shadow cover in mountainous

174　context.

175　　　We applied the L7/L8 correction method described by Roy et al. (2016a) to our data to align L8 reflectance to L7. No correction

176　was applied on L5 or L7 as it was shown that the surface reflectance products from Landsat Ecosystem Disturbance Adaptive Processing

177　System (LEDAPS) are consistent through time, with no difference before and after the 2003 ETM+ Scan-Line Corrector (SLC) failure. The

178　BRDF effects due to changes in solar and viewing zenith angle were corrected using the c-factor approach (Roy et al., 2016b) based on the

179　RossThick-LiSparse BRDF model (Schaaf et al., 2002) and using an optimal normalised solar zenith angle defined by Zhang et al. (2016).

180　We applied the Sun-Canopy-Sensor + C model (Soenen et al., 2005) on the recommendation of Sola et al. (2016) to correct for illumination

181　conditions variation due to slope and aspect. Finally, clouds were masked for each scene using the MFmask 4.0 algorithm

182　(https://github.com/gersl/fmask) using the default DEM and a cloud probability threshold of 40%. This version has improved clouds and

183　cloud shadows detection by integrating auxiliary data, new cloud probabilities and novel spectral-contextual features, which was crucial in

184　mountainous area where integration of global DEM to normalise thermal and cirrus bands is necessary (Qiu et al., 2017, Qiu et al., 2019a,

185　Qiu et al., 2019b, Zhu and Woodcock, 2014, Zhu and Woodcock, 2012). Masks were computed for cloud probability threshold of 10%, 40%

186 and 70% for a Landsat 7 ETM+ scene (195-029, captured the 16/07/2019) and visually compared to Fmask 3.3 (Figure S8). The probability
187 of 40% offered good compromise between omission and commission errors and was thus selected. A detailed correction workflow is
188 available in supplementary materials.

189   To assess vegetation changes at pixel-scale over the eight glacier forefields, we computed the NDVI as follows:

$$NDVI = \frac{(R_{NIR} - R_{Red})}{(R_{NIR} + R_{Red})}$$

191 where R_{NIR} and R_{Red} are the Normalised BRDF-adjusted and topographically corrected reflectance in the NIR and Red bands, respectively.
192 Then, we computed the NDVI annual maximum (NDVImax) available from 01 June to 31 August (day of year ~ 152 to 243) from 1984 to
193 2019 to obtain a time series of an indicator of vegetation state at 30-m scale. As shown by Berner et al (2020), it is challenging to reliably
194 estimate annual NDVImax using Landsat since these estimates are sensitive to the number of cloud- and snow-free observations acquired
195 each summer. Annual number of usable summer observations increased from 1984 to 2019, with typically few usable summer observations
196 during the 1980s and 1990s (Zhang et al. 2022). This bias results in a systematic underestimation of NDVImax when few observations are
197 available (Figure S9). To prevent related errors in NDVI trend estimation, a year is discarded from the pixel time series if the mean day of
198 year is superior/inferior to ±2σ of the entire time series as described in Bayle et al (2022) (Fig. S10).
199

200 **3. Statistical analysis**

201   Our data analysis workflow is based on using very high resolution chronosequence of deglaciation, Landsat time series and
202 vegetation surveys to derive three "early succession dynamics indicators". The heterogeneity of these indicators will be explored based on
203 "predictor variables" divided in two categories: the local environmental context and potential geomorphological disturbances. These analyses
204 intend to better understand the deterministic vs. stochastic nature of early succession dynamics in the theoretical framework proposed by
205 Wojcik et al. (2020). The complete workflow is presented in Figure 2.
206

207 *3.1. Remote sensing-based indicators of succession dynamics*

208   Based on the NDVImax time series, we characterized the proglacial vegetation dynamics at Landsat pixel-scale using two
209 indicators. The (i) Time Lag (TL_{NT}), i.e., the number of years between the Year of Deglaciation (YOD) and the year where the NDVI
210 threshold (NT) is exceeded (YOE_{NT}), and the (ii) Growth Rate (GR_{NT}), i.e., the NDVImax trends computed from the YOE_{NT} to the last year
211 of the Landsat time series. Ideally, we would compute both indicators for a NT that could identify the year of colonization by vegetation,
212 but as NDVI tends to show noise unrelated to vegetation and that plant establishment is a progressive phenomenon occurring at small scale
213 compared to pixel scale, such a threshold does not exist. Thus, we selected a NT based on Bayle et al. (2021). By comparing Landsat NDVI
214 values to intra-pixel vegetation cover derived from Unmanned Aerial Vehicle (UAV) image, they showed, for example, that a value of 0.071
215 efficiently discriminates pixels around 5% of vegetation cover (F-score > 0.75) with best efficiency with a value of 0.1 to discriminate with
216 more and less than 13% of vegetation cover (F-score > 0.85). Based on this work, we used an NT of 0.075 as it was a good compromise
217 between specificity and sensitivity regarding plant cover.
218   Thus, we used $TL_{0.075}$ and $GR_{0.075}$ to quantify heterogeneity of intra- and inter-glacier forefield succession dynamics. To consider
219 a year as the one where the NT is exceeded, the NDVI of the two previous years must be lower, and the two next years to be higher. Theil-
220 Sen trend estimator was applied for $GR_{0.075}$ estimation as it is resistant to outliers in short or noisy series (Eastman et al., 2009). An example
221 of an NDVI time series and all associated data is shown in Figure 3A. We evaluated our method by comparing plant cover (%) obtained

from field sampling between plots identified as vegetated or unvegetated. Finally, as the Landsat time series is limited to the last 40 years, there is a bias in the $TL_{0.075}$ value as it is directly constrained by the YOD. For example, a pixel deglaciated in 2010 could only be colonized in the 9 following years, thus limiting the absolute value of $TL_{0.075}$ between 1 and 9 years. To bypass this bias, we computed the anomalies of $TL_{0.075}$ and $GR_{0.075}$ as a function of YOD, which is a more relevant measure of heterogeneity in succession dynamics across the eight glacier forefields (Fig. 3B and 2C).

Finally, we implemented two random forest classification analyses to assess relationships between anomalies of $TL_{0.075}$ and $GR_{0.075}$ and predictors (Breiman, 2001). We classified the two indicators into three categories: positive anomalies (anomalies of $TL_{0.075}$ | $GR_{0.075}$ > 0), negative anomalies (anomalies of $TL_{0.075}$ | $GR_{0.075}$ < 0) and no vegetation detected. For TL, it resulted in 337, 374 and 1977 samples for positive, negative and no detection, respectively, and for GR, 441, 288 and 1959 samples for positive, negative and no detection, respectively. Only 337 and 288 samples were conserved for TL and GR, respectively, to equalize the sample size of each class.

Predictors variables included (i) elevation, (ii) local vegetation and (iii) snow-free growing degree days (SF-GDD) to represent the environmental context (allogenic factors) of the glacier forefields. Elevation was obtained from the 25-m resolution European Digital Elevation Model (EU-DEM, version 1.1; https://land.copernicus.eu/imagery-in-situ/eu-dem/). Snow-free growing degree days (SF-GDD) maps were calculated through the combined use of the Snow-melt out date (SMOD) product at 20-m resolution derived from Sentinel-2 time series analysis (Gascoin et al., 2019, Barrou Dumont et al., 2021), and the SAFRAN-CROCUS climatological model from Météo-France (Vernay et al., 2022), which provides the average daily temperature for each French massif and for 300 m elevation bands (for Swiss and Italian sites, we applied data from the French Mont-Blanc and Vanoise massifs, respectively). To obtain the SF-GDD for each plot, we computed the cumulative sum of daily average air temperature above 0°C between snow melt-out date and August 1 for the year 2019. SF-GDD is representative of the heat accumulated by vegetation during the growing season and is known to be a key variable for habitat distribution and alpine plant community properties (Choler, 2015, Choler, 2018, Carlson et al., 2015). We defined local vegetation surrounding the glacier forefield as the expected local vegetation productivity (NDVImax) for a given elevation outside of the glacier forefield, which we considered to be a proxy of the vegetation proximity and type. To compute this indicator for each plot, we averaged the NDVImax of the year of deglaciation for the 100-m elevational bands of the plot within a radius of 500-m and by excluding pixels within the glacier forefield.

We also calculated (i) Flow accumulation and (ii) LS-factor (slope length and steepness-Factor) to represent potential geomorphological disturbances (allogenic factors). The LS factor was derived from the EU-DEM and computed using the original equation proposed by Desmet and Govers (1996). It combined the S-factor, which accounts for slope angle, and the L-factor that defines slope length. The combined LS-factor describes the effect of topography on soil erosion and thus is a proxy of "potential" instability due to gravity-related processes. Flow accumulation was also derived from the EU-DEM and computed using a Multiple Flow Direction algorithm. Both the LS-factor and Flow accumulation were computed in SAGA (Conrad et al., 2015).

We screened highly correlated variables ($r^2 > |0.7|$) by computing pairwise correlations. We then removed elevation as it was highly correlated to SF-GDD (r^2=-0.73) and Local vegetation (r^2=-0.84). Next, we randomly partitioned the data set into sets for model training (two-thirds) and evaluation (one-third), and then fit random forest models to optimize out-of-bag classification accuracy. We reassessed the classification accuracy using the data withheld for model evaluation. We repeated this operation 100 times. Lastly, we computed predictor importance using the mean decrease in accuracy metric. Predictor importance was calculated using a permutation-based importance measure where one measures the effect of reshuffling each predictor on model accuracy. Finally, we generated partial dependence plots for the first variable in terms of importance as defined above to assess how class-specific classification probabilities varied across the range of the predictor while holding all other predictors at their average value. The distribution of predictors was constrained to regions with enough data

260 given that partial dependence plots tend to overinterpret regions with few observations. We used the random Forest, caret, and pdp R
261 packages to implement random forest models and to evaluate their performance (Liaw and Wiener, 2002, Greenwell, 2017).
262
263 *3.2. Heterogeneity of succession dynamics and drivers*

264   To model succession dynamics from the floristic data, we used Non-metric Multidimensional Scaling (NMDS) to perform an
265 unconstrained ordination of the plot by species table. NMDS is a rank-order based multivariate technique that is particularly robust to identify
266 a few important axes of floristic variations in community composition data (Minchin, 1987). We first discarded species with less than five
267 occurrences to limit the proportion of sites with no shared species, as this may complicate the ordination. The resulting table included a total
268 of 297 plots and 119 species. Absolute cover of plant species was transformed into relative species cover using the Wisconsin standardisation,
269 where species covers are first standardised by maxima and then site covers by maxima. Finally, we calculated the square root of relative
270 plant cover for each species and for each plot. These transformations are commonly found to improve the results of the NMDS (Legendre
271 and Gallagher, 2001). We then computed a distance matrix using the Bray-Curtis dissimilarity index on transformed species cover with 2
272 dimensions and 20 minimum random starts iterated two times. To avoid local minima, we performed several NMDS with random starts and
273 selected the solution with the minimum stress, i.e., the extent to which the distance between sites in the specified number of dimensions
274 differs from original distances. We used a vector fitting approach to test for linear relationships between NMDS site scores and two sets of
275 variables corresponding to allogenic factors (neighbouring vegetation cover, SFGDD, elevation) and geomorphological context (LS-factor,
276 flow accumulation and coarse debris). To account for spatial autocorrelation, we implemented two generalized least square (GLS) regression
277 models for each variable: one including an autocorrelated error structure and one without. We used the spherical spatial correlation structure
278 estimated by the function corSphere in the nlme package (Pinheiro and Bates, 2022). The best fitting model was selected using the Akaike
279 Information Criterion corrected for small sample size (AICc). For each competing model, we estimated a pseudo-R-squared based on the
280 regression of the variable on the fitted values. NMDS was performed using the metaMDS function of the vegan R package (Oksanen et al.,
281 2020). GLS regression was fitted using the gls function of the nlme R package. Model evaluation was performed with the R package MuMIn
282 (Barton, 2023) . In addition to environmental context and potential disturbance regime variables (allogenic factors) presented in section 3.1,
283 we also considered sediment granulometry as measured in the field with floristic data. Using visual estimates of substrate type and cover
284 carried out for each floristic plot, we calculated a cumulative weighted mean for each plot of grain size (sand < 0.5 cm, gravel < 2 cm,
285 cobbles between 2 and 20 cm and boulders between 20 cm and 1 m in diameter) by assigning the median value for each class and calculating
286 a cumulative weighted mean.
287

288 **4. Results**

289 *4.1. Vegetation dynamics heterogeneity assessed through remote sensing*

290   Using 36 years of NDVImax obtained from the Landsat time series, we found strong heterogeneity within and between glacier
291 forefields. It took on average 10 years following deglaciation to reach an average NDVI value of 0.075 for GB in comparison with, for
292 example, 27 years for GEB, 17 for TR, 25 for STS, or even no vegetation detected for LAU over the entire period (Fig. 4). Within glacier
293 forefields, plant colonisation rates varied depending on the glacier with GB depicting the highest heterogeneity in NDVI dynamics following
294 deglaciation, and TR being the more homogenous with almost no pixel with an NDVI value under 0.075 after 30 years (Fig. 4). Also, we
295 did not find vegetated pixels for LAU over the study period, which was corroborated by low plant cover recorded in the 2019 field survey

296   (on average 4%). By simply considering pixels as colonised by plants or not, we found that after 30 years since deglaciation 80% of GB,

297   TR, and STS forefields were colonised, and only 30% for PEL and LAV (Fig. 5). Overall, considering anomalies of TL0.075, we found

298   similar results with GB being the most dynamic forefield with pixels that tended to become colonised by vegetation three years faster and

299   with higher growth rates than average (Fig. 6A).

300   The two random forest models achieved an overall accuracy of 75% and 72% for TL and GR respectively, which translated a good

301   capacity of the four predictors to classify time lag and growth rate anomalies as positive, negative, or absent. Mean decrease in accuracy

302   (MDA) was used to order the four predictors according to their importance of overall classification accuracy (Fig. 7). SF-GDD was overall

303   the most important predictor for both models (MDA = 0.128 [0.127] for TL [GR]) compared to Local vegetation, LS-factor, and Flow

304   accumulation (respectively, 0.062 [0.052], 0.051 [0.041] and 0.044 [0.04] for TL [GR]). Overall, allogenic factors describing environmental

305   context were more important than potential geomorphological disturbances variables (Fig. 7A and 7B). Classification probabilities showed

306   that faster colonisation occurred with SF-GDD > 900 (Prob > 0.5) while slower colonisation occurred mostly between 500 and 900 SF-

307   GDD. Slower growth rates occurred with SF-GDD > 500 while faster growth rate occurred sporadically above 900 SF-GDD (Fig. 7D). The

308   class of undetected vegetation occurs mostly under 500 SF-GDD for both TL and GR (Fig. 7C and 7D).

309

310   *4.2. Agreement between field and Landsat observations of plant cover*

311   By comparing plant cover of the 297 floristic plots to the detection of vegetation as detected by Landsat NDVI, we found that the

312   221 floristic plots identified as unvegetated had an average plant cover of 5% (Fig. 6C). These results matched the initial sensitivity targeted

313   considering the scale difference between Landsat pixel and floristic plots. Similarly, we found anomalies of TL0.075 and GR0.075 to be

314   representative of the overall vegetation dynamics of glacier forefields as values tended to be similar when we compared only pixels that

315   overlapped floristic plots to the entire forefield (Fig. 6A and 6B).

316

317   *4.3. Environmental context drives plant species assemblages and succession dynamics*

318   The first axis of the NMDS showed a floristic gradient representative of species turnover along an elevation gradient throughout

319   the southwestern European Alps (Fig. 8A and 8B). Cold-adapted high alpine specialist species, included low-stature, pioneer

320   hemicryptophytes of sparsely vegetated screes, talus, and rock debris such as *Linaria alpina*, *Cerastium uniflorum* and *Saxifraga spp.* Species

321   typically found at lower elevations, included phanerophytes (*Picea abies*) and chamaephytes (*Vaccinium uliginosum*). Notably early

322   successional species in the context of the Glacier Blanc, Pèlerins, and Tour glaciers included trees and shrubs such as *Larix decidua* and

323   *Salix laggeri*.

324   The GLS model including a spatial correlation error structure had better fit (lower AICc) for the three allogenic variables and for

325   flow accumulation. The importance of the spatial structure was particularly strong for elevation with a pseudo-R2 of 0.74 without spatial

326   autocorrelation to be compared to 0.23 with spatial autocorrelation. This indicated that the relationship between elevation and the floristic

327   composition was mainly driven by the elevational differences between glacier forefields. For all other variables, we found no major changes

328   in the relationships between NMDS axes and variables. NMDS1 was positively correlated to neighbouring vegetation cover (pseudo R-

329   squared=0.629) and SF-GDD (pseudo R^2=0.559) in the best fit models. NMDS1 was poorly correlated to other factors such as the LS factor

330   (r^2=0.25), debris size (r^2=0.0836), Flow accumulation (r^2=0.037) and time since deglaciation (r^2=0.0046). By comparing NMDS1 scores to

331   time since deglaciation, we found that elapsed time following deglaciation led to more late successional species for all glacier forefields

(except PEL) but at a rate insufficient to surpass the effect of initial plant community composition (Fig. 9). We found that the initial starting point of the succession to be mostly driven by allogenic factors describing the environmental context (average $r^2=0.68$), and not potential geomorphological disturbances (average $r^2=0.1288$) or time available ($r^2=0.0046$) (Table 1). Finally, we found that the heterogeneity of vegetation dynamics described through the anomalies of TL0.075 and GR0.075 were linked to the NMDS1 scores with slower colonisation (positive TL0.075 anomalies) and growth (negative GR0.075 anomalies) rate corresponding to lower NMDS1 site scores (Figure 10).

5. Discussion

Our comparative study of vegetation dynamics in glacier forefields based on two complementary and independent approaches provides insight into the heterogeneity of early plant succession dynamics after glacier retreat at the regional scale. First, using the Landsat time series, we found strong variability in the time lag between deglaciation and colonisation by plants and plant growth rate within and between glacier forefields (Fig. 4, 5 and 6). We showed that this heterogeneity was mostly explained by the local environmental context, i.e., local vegetation surrounding the forefields and energy availability linked to temperature and snowmelt gradients, rather than potential geomorphological context (Fig. 7). Furthermore, we found that the composition of early plant succession communities (0-35 years since deglaciation), i.e., the initial starting point of plant succession, was highly variable from one glacier to another, and depended strongly on the topoclimatic context of the glacier forefield (Fig. 8 and Tab. 1). Interestingly, elapsed time since deglaciation was insufficient to overstep the determinism of the initial starting point, highlighting the importance of the local environmental context to understand early plant succession in glacier forefields (Fig. 9). Overall, both approaches converged towards this conclusion (Fig. 10) suggesting that early plant succession is not stochastic as previous authors have suggested (Wojcik et al., 2021) but rather deterministic in relation to environmental conditions.

5.1. Succession dynamics in glacier forefields are shaped by local environmental context

In our analysis, early vegetation dynamics in glacier forefields can be divided into two phases: (i) the lag between deglaciation and plant colonisation(as detected by satellite); and (ii) the succession dynamics following initial plant colonisation (Fig. 3). We analyzed the heterogeneity of the first phase through two approaches based on remote sensing. First, as we distinguished vegetated from non-vegetated pixels, we were able to estimate the proportion of glacier forefields to become colonized by vegetation with respect to time since deglaciation. We found strong heterogeneity between glacier forefields, with 80% of the forefield colonized by plants after 30 years for GB, TR, and STS, while the five other forefields did not reach 50% of vegetation cover over the same period, with no vegetation identified for LAU (Fig. 5). The second approach directly quantifies the time lag between deglaciation and plant colonisation. Nonetheless, as the range of absolute time lag is constrained by the length of the period between the year of deglaciation and the end of the time series, time lag could only be compared as anomalies regarding the median time lag for each year of deglaciation (Fig. 7A).

Time lag between deglaciation and plant establishment has been shown to be dependent on the proximity and availability of seed sources (Erschbamer et al., 2001, Stöcklin and Bäumler, 1996, Tackenberg and Stöcklin, 2008; Garbarino et al. 2010) and species ability to disperse (Fickert and Grüninger, 2018), findings which are consistent with our results. Indeed, using partial dependency analysis, we showed that the time lag anomalies (including the absence of vegetation detected) are distributed along the SF-GDD gradient, which in turn is highly correlated to both elevation and neighbouring vegetation cover. These results confirm that high elevation forefields surrounded by sparsely vegetated scree slopes tend to be colonized more slowly than forefields at lower elevation with dense patches of vegetation nearby. This conclusion is supported if we consider the most and least dynamic forefields (in terms of vegetation colonization rate), respectively GB and

10

369   LAU, which match these characteristics. In terms of spatial distribution, the GB forefield is also located at lower latitude and is the only
370   south facing glacier forefield among the eight glaciers studied (Fig. 1), both of which contribute to earlier snowmelt-out and greater
371   accumulation of growing degree days for an equivalent elevation located on a north-facing glacier situated at a higher latitude. Indeed, the
372   left bank of the GB forefield has been described by Bayle (2020) as highly dynamic, which is confirmed here with colonization occurring
373   within 1 to 5 years after deglaciation, as reported elsewhere in the European Alps (Burga et al., 2010, Cannone et al., 2007, Fickert and
374   Grüninger, 2018). This specificity is known to be due to the proximity of a dense vegetation patch which was located at less than 100 m to
375   the glacier tongue in 1984 and at low elevation (2400 m a.s.l.). Conversely, the LAU forefield deglaciated at the same period is located at
376   3100 m a.s.l., further to the north in the Grand Paradiso National Park with only sparse vegetation nearby (Mainetti et al., 2021).

377   While previous studies have reported consistent pioneer plant species and functional groups giving way to later successional
378   species in the context of glacier forefields (e.g. Shumann et al. 2016), our study of multiple glacier forefields indicates that the identity of
379   pioneer species varies highly from one site to another and depends strongly on local environmental context. Figure 9 shows that practically
380   all of the plant communities encountered across the floristic gradient of the eight forefields have the potential to be pioneer species, given
381   the wide range of initial starting points for initial community composition shown across NMDS scores. We emphasize that tree species such
382   as *Picea abies* or *Betula pubescens*, or shrubs such as Salix laggeri, are just as capable of establishing quickly in the wake of glacier retreat
383   as smaller stature forbs including Saxifraga or Poa spp. (Figure 8-9). Accordingly, we argue that the identity of pioneer species and the
384   structure of community composition, as well as the subsequent rate of growth following establishment (Fig. 10), are strongly influenced
385   during the first decades of succession by energy availability and nearby vegetation.

386

387   *5.2. The importance of geomorphological drivers of plant succession dynamics*

388   While we did not observe high explanatory power of geomorphic variables in explaining the heterogeneity of succession dynamics
389   in glacier forefields, a large number of studies have shown otherwise (Gurnell et al., 2001, Moreau et al., 2008, Burga et al., 2010, Eichel et
390   al., 2013, Temme and Lange, 2014, Klaar et al., 2015, Heckmann et al., 2016, Eichel et al., 2018, Eichel, 2019, Miller and Lane, 2018,
391   Wojcik et al., 2020, Wojcik et al., 2021). Biogeomorphological studies emphasise that landscape dynamics within glacier forefields depend
392   on the balance between stabilising and destructive forces (Eichel et al., 2018). Indeed, proglacial plant succession in the wake of deglaciation
393   alters site conditions and decreases the magnitude and/or the spatial extent of geomorphological disturbances (Gurnell et al., 2000, Moreau
394   et al., 2008, Eichel, 2019, Miller and Lane, 2018). More specifically, the biogeomorphic phase, characterized by feedbacks between abiotic
395   and biotic processes, is a key stage of landscape stabilisation in glacier forefields. However, exacerbated fluvioglacial and hillslopes
396   processes within the deglaciated area during the first stage of the so-called paraglacial period may also delay the succession rate through
397   rejuvenation of proglacial deposits (Wojcik et al., 2020).

398   Through the remote sensing and floristic approaches used here, GB displayed exceptionally fast colonisation in certain areas but
399   also high heterogeneity within the forefield, with up to 30 years of difference in time lag for the same year of deglaciation (Fig. 6A). We
400   attribute this heterogeneity to spatial variability in the intensity of potential geomorphological disturbance (Lardeux et al., 2015).
401   Specifically, a gullying area on the right bank of the forefield remains active and thus prevents vegetation establishment, as described by
402   Bayle (2020) and Lardeux et al. (2015). This geomorphic activity is known to be the result of an active eroding slope supported by a slowly
403   melting ice-cored moraine, which is a phenomenon too fine and complex to be captured by our low-resolution variables of potential
404   instability. This example shows that, although the sum of degree days during the growing season (SF-GDD) and local vegetation explained
405   most of the observed heterogeneity in observed vegetation dynamics (lag and growth rate), finer variables estimating direct instability and

11

geomorphic activities based on a high-resolution imagery or field measures would locally change the balance of importance and improve the predictive capacity of models (Fig. 7). The PEL glacier provides a further example, where we observed long lag times and slow growth rates despite relatively low elevation and accordingly high SF-GDD, which we attribute to the extremely chaotic and blocky substrate observed in the field. Although we did attempt to capture potential geomorphological disturbances through substrate heterogeneity by calculating the weighted mean estimate of block size for floristic plots, we found similar results in this case compared to coarser DEM-based variables. Thus, we lacked a spatially continuous and ecologically relevant estimate of substrate properties. Estimating block size and geomorphological properties using a remote sensing approach has been explored (Westoby et al., 2017, Vázquez-Tarrío et al., 2017, Langhammer et al., 2019, Eichel et al., 2020, Lang et al., 2021) and constitutes an important perspective for enhancing the analysis conducted in the present study, perhaps especially in regard to later plant succession dynamics known to be particularly linked to biogeomorphic feedbacks (Eichel et al., 2016, Miller and Lane, 2018, Lane et al., 2016).

We argue that the poor predictive capabilities of our geomorphological variables can be in part explained by the fact that those measures potential and not realised instability. Furthermore, the poor predictive capacity of our potential geomorphological disturbance variables could be explained by scale differences. Most studies highlighting the importance of geomorphic activities in explaining succession dynamics heterogeneity have been conducted at the glacier forefield scale at sub-meter spatial resolution. Our regional-scale approach showed that the local environmental context drives an initial starting point and that other local factors are insufficiently determinant to overrule it (Fig. 9   ). We hypothesise that for our analysis, the importance of geomorphological variables and processes were overshadowed by broader-scale and more contextual drivers such as energy availability. Finally, because of the low sensitivity of our remote sensing approach (discriminating vegetation cover around 10% only), it is possible that we only detect vegetation that develops on stable surfaces unaffected by geomorphological activities. In other words, we might only detect vegetation after the battle between substrate instability and colonization by plants (Eichel et al. 2016), resulting in large underestimation of the importance of geomorphological activities.

5.3. The Landsat time series effectively captures vegetation dynamics in a real-time approach

The Landsat time series offers the possibility to study vegetation dynamics using a real-time approach, given its temporal resolution and depth (Wulder et al., 2019, Bayle et al., 2021). For the first time, we used the Landsat archive since the mid-1980s to quantify real-time plant colonization dynamics at the scale of glacier forefields, based on ecologically relevant indicators of time lag and growth rate following establishment. In the context of the observed generalized greening of the European Alps (Choler et al. 2021), these parameters provide further insight into trajectories of plant colonization in the context of peri   glacial greening hotspots. Nonetheless, this approach inevitably comes with some uncertainty and bias that merit discussion.

Relationships between NDVI and certain biophysical properties of vegetation canopies, such as leaf area index (LAI), vegetation cover and biomass have been widely studied (Ormsby et al., 1987, Wittich and Hansing, 1995), including in the context of glacier forefields (Bayle et al., 2021, Knoflach et al., 2021) and in sparsely vegetated sites in the Antarctic (Fretwell et al., 2011). Further testing of relationships between NDVI and plant canopy properties in the context of glacier forefields remains necessary, however, to better understand the effects of specific conditions unrelated to vegetation that can alter reflectance, such as low organic content in soil (Todd et al., 1998), coarse granulometry and complex angular effects due to micro-topography (Bayle et al., 2021). Despite the difference in area between field plots (2x2m) and Landsat pixels (30x30m), we found similar sensitivity between ground truth vegetation cover and NDVI values to that of Bayle et al. (2021) and thus validate that within this study region an NDVI value of 0.075 efficiently identifies pixels with more of less than 5-10% of vegetation cover (Figure S10). Nonetheless, because of coarse resolution and noises inherent to NDVI time series, our approach is

443 unable to detect reverse trends with vegetated pixels changing to unvegetated pixels. For example, after several years of vegetation detection,

444 a sudden drop in NDVI resulting in the pixel being identified as unvegetated could be interpreted as the result of disturbance or due to

445 spectral-related noises, with no possibilities to decipher one from another. Improvement of our approach could be done by using proper

446 ground control information regarding abrupt disturbances in glacier forefields. Also, systematic UAV flight on each glacier forefield could

447 drastically improve the calibration of satellite remote sensing methods while providing relevant information on vegetation distribution and

448 geomorphic activities at one time (Woellner & Wagner, 2019; Healy & Khan, 2022; Lang et al. 2021; Westoby et al. 2017).

449   Finally, we found that to take full advantage of the time series, the presence of clouds was problematic as the actual cloud mask

450 applied in the data distributed by the USGS (Fmask 3.3) is inefficient in high elevation areas as soil temperature is too low and is often

451 confused with clouds (Qiu et al., 2017, Qiu et al., 2019b). Thus, we recommend using the modified MFmask 4.0 to improve the number of

452 images available (Figure S8). Despite these challenges, our study thus confirms that the Landsat time series can be efficiently used to monitor

453 vegetation cover changes over time in the context of glacier forefields.

454

455

456 *5.4. Field sampling recommendations*

457   Several studies have shown that the initial site conditions defined by substrate material, topography, micro-climate, landscape

458 surroundings, as well as by varying frequencies and/or magnitudes of natural disturbances between sites, are of high importance in

459 determining plant succession dynamics in glacier forefields (Joly and Brossard, 2007, Walker and Wardle, 2014, Wojcik et al., 2020, Eichel

460 et al., 2016). Repeated visits of permanent plots represent an alternative to the regular space-for-time approach as they provide a more

461 informative and reliable measure of succession. This approach is costly in terms of effort, however, and furthermore it can be difficult to

462 mark permanent plots in unstable terrain often found in glacier forefields (but see Bakker et al., 1996). An intermediate and less-costly

463 approach consists in measuring variations in initial site conditions and geomorphological disturbances along the chronosequence, as proposed

464 by Wojcik et al. (2021). In our field campaign, the eight glacier forefields were surveyed based on a random sampling approach along the

465 chronosequence of deglaciation, however vegetation plots captured overall heterogeneity within forefields with varying degrees of success

466 (Fig. 6). In accessible glacier forefields of small size and limited geomorphic activities (TR, PEL, GEB, STS and OR), our approach worked

467 as floristic plots were found to be representative of the vegetation dynamics as assessed from the spatially exhaustive remote sensing

468 approach (Fig. 6). The representativity was less evident for LAV, which can be explained by the large size of the forefield and the presence

469 of cliffs and a lake that drastically constrained accessibility. Also, surfaces known to be affected by geomorphological activities might have

470 been under sampled as for example the field sampling on GB forefield was mostly limited to the left bank as the right bank was too dangerous

471 due to gullies and ice-cored moraines (Lardeux et al. 2015; Bayle 2020). Noticeably, our results show that the within forefield variability in

472 vegetation dynamics can be equivalent to the variability observed at regional scale, thus leading to massive bias in our capacity to extrapolate

473 results when studies rely solely on a space-for-time approach applied to a single glacier forefield.

474   Our study provides lessons that could contribute toward improving future studies carried out in glacier forefields. Although

475 explaining the absence of vegetation was not our question here, to understand where plants will establish, we recommend sampling points

476 characterised by an absence of vegetation in addition to vegetated areas. Indeed, the first step in the primary succession dynamics is whether

477 vegetation can colonise a surface. Thus, the absence of vegetation on deglaciated surfaces should be considered as an extreme case of equal

478 ecological relevance as vegetated plots, especially in the context of biogeomorphic feedbacks and regular disturbances minimising the

479 probability of establishment and germination. Thus, in the perspective of an exhaustive and representative sampling of the glacier forefield,

13

480 collecting information on the absence of vegetation appears to be crucial for future field campaigns. Overall, we recommend the following
481 procedure for future field campaigns:

482 (1) Randomly select a predefined number of points using GIS software within targeted glacier forefields.

483 (2) Collect information unrelated to vegetation on plots whether there is vegetation or not and keep track of unreachable random points
484 due to dangerous access as it is a marker of high geomorphic activity, and select plot size and location to facilitate alignment with satellite
485 imagery.

486 (3) Measure plant community structure and composition, including functional traits, both within and outside of the glacier forefields
487 to capture the local environmental context through field sampling.

488

6. Conclusion

490   We quantified heterogeneity in plant succession dynamics based on 36 years of optical satellite imagery and 297 floristic plots
491 distributed among eight glacier forefields in the southwestern European Alps. The projection of autogenic and allogenic factors according
492 to the definition presented in Wojcik et al. (2021) shows that the pioneer plant community composition is strongly correlated with
493 environmental context rather than time since deglaciation. Time since deglaciation is typically identified as the main driver of succession
494 dynamics, as it is fundamentally intrinsic to the idea of succession. Nonetheless, whether time since deglaciation is identified as the main
495 driver of succession is a matter of scale. We showed that, indeed, if we consider each forefield independently, a clear successional gradient
496 emerges as time since deglaciation increases. But when considering all eight glacier forefields together, energy availability and initial species
497 composition emerged as the key parameters shaping successional dynamics. In the case of both remotely sensed vegetation indices and plant
498 field surveys, we found that this initial starting point was strongly correlated to the local environmental context, rather than the
499 geomorphological context, suggesting that the notion of a "pioneer" species is actually quite flexible (Table 1). Overall, our findings suggest
500 that early stages of plant succession in glacier forefields in the European Alps are highly dependent on the local environmental context and
501 less stochastic than previous studies have suggested.

502   In the conceptual framework of Wojcik et al. (2021), our findings suggest a reinterpretation of the importance of local
503 environmental context in the initial stages of primary succession, which is considered to be highly stochastic (Chase and Myers, 2011, Dini-
504 Andreote et al., 2015, del Moral, 2009, Mong and Vetaas, 2006, Marteinsdóttir et al., 2010). In contrast, we found that this initial phase was
505 driven by plant opportunism originating from neighbouring vegetation, which is a function of environmental context and other biogeographic
506 factors. We highlighted that for the first 30 years of succession, initial plant community composition was far more important than time since
507 deglaciation in shaping plant assemblages and rates of colonization, thus pointing to the importance of quantifying more direct drivers of
508 succession dynamics including both environmental and biological factors. Our work highlights the ongoing need for process-based studies
509 combining remote sensing and field techniques to improve our understanding of local heterogeneity in plant colonisation trajectories, and
510 furthermore provides a promising basis for predicting future trajectories of plant succession in the wake of ongoing glacier retreat during the
511 coming decades using widely available remotely sensed predictors.

512

Data availability

514 Research data can be accessed upon request to the corresponding author. Part of the data used in this paper remains under exclusivity as it
515 was obtained through multiple programs and partnerships.

516

Author contribution

Conceptualisation AB and BC **Data curation** All authors contributed **Formal analysis** AB and BC **Writing – Original draft and preparation** AB and BC **Writing – review and editing** All authors contributed

Competing interests

The authors declare no competing interests.

References

Anthelme, F., Cauvy-Fraunié, S., Francou, B., Cáceres, B. & Dangles, O. 2021. Living at the Edge: Increasing Stress for Plants 2–13 Years After the Retreat of a Tropical Glacier. *Frontiers in Ecology and Evolution,* 9.

Bakker, J. P., Poschlod, P., Strykstra, R. J., Bekker, R. M. & Thompson, K. 1996. Seed banks and seed dispersal: important topics in restoration ecology§. *Acta Botanica Neerlandica,* 45**,** 461-490.

Barrou Dumont, Z., Gascoin, S., Hagolle, O., Ablain, M., Jugier, R., Salgues, G., Marti, F., Dupuis, A., Dumont, M. & Morin, S. 2021. Brief communication: Evaluation of the snow cover detection in the Copernicus High Resolution Snow & Ice Monitoring Service. *The Cryosphere,* 15**,** 4975-4980.

Bayle, A. 2020. A recent history of deglaciation and vegetation establishment in a contrasted geomorphological context, Glacier Blanc, French Alps. *Journal of Maps,* 16**,** 766-775.

Bayle, A., Roussel, E., Carlson, B. Z., Vautier, F., Brossard, C., Fovet, E., De Bouchard D'aubeterre, G. & Corenblit, D. 2021. Sensitivity of Landsat NDVI to subpixel vegetation and topographic components in glacier forefields: assessment from high-resolution multispectral UAV imagery. *Journal of Applied Remote Sensing,* 15.

Bayle, A., Roy, A., Dedieu, J.-P., Boudreau, S., Choler, P. & Lévesque, E. 2022. Two distinct waves of greening in northeastern Canada: summer warming does not tell the whole story. *Environmental Research Letters,* 17**,** 064051.

Barton, K. 2023. MuMIn: Multi-Model Inference. R package version 1.47.2/r505, https://R-Forge.R-project.org/projects/mumin/.

Bradshaw, A. D. 1993. Restoration Ecology as a Science. *Restoration Ecology,* 1**,** 71-73.

Breen, K. & Lévesque, E. 2008. The Influence of Biological Soil Crusts on Soil Characteristics along a High Arctic Glacier Foreland, Nunavut, Canada. *Arctic, Antarctic, and Alpine Research,* 40**,** 287-297.

Breiman, L. 2001. <Breiman2001_Article_RandomForests.pdf>. *Machine Learning,* 45**,** 5-32.

Burga, C. A., Krüsi, B., Egli, M., Wernli, M., Elsener, S., Ziefle, M., Fischer, T. & Mavris, C. 2010. Plant succession and soil development on the foreland of the Morteratsch glacier (Pontresina, Switzerland): Straight forward or chaotic? *Flora - Morphology, Distribution, Functional Ecology of Plants,* 205**,** 561-576.

Cannone, N., Sgorbati, S. & Guglielmin, M. 2007. Unexpected impacts of climate change on alpine vegetation. *Frontiers in Ecology and the Environment,* 5**,** 360-364.

Carlson, B. Z., Choler, P., Renaud, J., Dedieu, J. P. & Thuiller, W. 2015. Modelling snow cover duration improves predictions of functional and taxonomic diversity for alpine plant communities. *Annals of Botany,* 116**,** 1023-34.

Carlson, B. Z., Corona, M. C., Dentant, C., Bonet, R., Thuiller, W. & Choler, P. 2017. Observed long-term greening of alpine vegetation— a case study in the French Alps. *Environmental Research Letters,* 12**,** 114006.

Cauvy-Fraunie, S. & Dangles, O. 2019. A global synthesis of biodiversity responses to glacier retreat. *Nat Ecol Evol,* 3**,** 1675-1685.

Chapin, F. S., Walker, L. R., Fastie, C. L. & Sharman, L. C. 1994. Mechanisms of Primary Succession Following Deglaciation at Glacier Bay, Alaska. *Ecological Monographs,* 64**,** 149-175.

Chase, J. M. & Myers, J. A. 2011. Disentangling the importance of ecological niches from stochastic processes across scales. *Philosophical Transactions of the Royal Society of London B Biological Sciences,* 366**,** 2351-63.

Choler, P. 2005. Consistent Shifts in Alpine Plant Traits along a Mesotopographical Gradient. *Arctic, Antarctic, and Alpine Research,* 37**,** 444-453.

Choler, P. 2015. Growth response of temperate mountain grasslands to inter-annual variations in snow cover duration. *Biogeosciences,* 12**,** 3885-3897.

Choler, P. 2018. Winter soil temperature dependence of alpine plant distribution: Implications for anticipating vegetation changes under a warming climate. *Perspectives in Plant Ecology, Evolution and Systematics,* 30**,** 6-15.

Choler, P., Bayle, A., Carlson, B. Z., Randin, C., Filippa, G. & Cremonese, E. 2021. The tempo of greening in the European Alps: Spatial variations on a common theme. *Global Change Biology,* 27**,** 5614-5628.

568   Conrad, O., Bechtel, B., Bock, M., Dietrich, H., Fischer, E., Gerlitz, L., Wehberg, J., Wichmann, V. & Böhner, J. 2015. System for
569   Automated Geoscientific Analyses (SAGA) v. 2.1.4. *Geoscientific Model Development,* 8**,** 1991-2007.

570   Del Moral, R. 2009. Increasing deterministic control of primary succession on Mount St. Helens, Washington. *Journal of Vegetation Science,*
571   20**,** 1145-1154.

572   Desmet, P. J. J. & Govers, G. 1996. A GIS procedure for automatically calculating the USLE LS factor on topographically complex landscape
573   units. *Journal of Soil and Water Conservation,* 51.

574   Dini-Andreote, F., Stegen, J. C., Van Elsas, J. D. & Salles, J. F. 2015. Disentangling mechanisms that mediate the balance between stochastic
575   and deterministic processes in microbial succession. *Proceedings of the National Academy of Sciences of the United States of*
576   *America,* 112**,** E1326-32.

577   Eastman, J., Sangermano, F., Ghimire, B., Zhu, H., Chen, H., Neeti, N., Cai, Y., Machado, E. A. & Crema, S. C. 2009. Seasonal trend
578   analysis of image time series. *International Journal of Remote Sensing,* 30, 2721-2726.

579   Eichel, J. 2019. Vegetation Succession and Biogeomorphic Interactions in Glacier Forelands. 327-349.

580   Eichel, J., Corenblit, D. & Dikau, R. 2016. Conditions for feedbacks between geomorphic and vegetation dynamics on lateral moraine slopes:
581   a biogeomorphic feedback window. *Earth Surface Processes and Landforms,* 41**,** 406-419.

582   Eichel, J., Draebing, D., Kattenborn, T., Senn, J. A., Klingbeil, L., Wieland, M. & Heinz, E. 2020. Unmanned aerial vehicle-based mapping
583   of turf-banked solifluction lobe movement and its relation to material, geomorphometric, thermal and vegetation properties.
584   *Permafrost and Periglacial Processes,* 31**,** 97-109.

585   Eichel, J., Draebing, D. & Meyer, N. 2018. From active to stable: Paraglacial transition of Alpine lateral moraine slopes. *Land Degradation*
586   *& Development,* 29**,** 4158-4172.

587   Eichel, J., Krautblatter, M., Schmidtlein, S. & Dikau, R. 2013. Biogeomorphic interactions in the Turtmann glacier forefield, Switzerland.
588   *Geomorphology,* 201**,** 98-110.

589   Erschbamer, B., Kneringer, E. & Schlag, R. N. 2001. Seed rain, soil seed bank, seedling recruitment, and survival of seedlings on a glacier
590   foreland in the Central Alps. *Flora,* 196**,** 304-312.

591   Ficetola, G. F., Marta, S., Guerrieri, A., Gobbi, M., Ambrosini, R., Fontaneto, D., Zerboni, A., Poulenard, J., Caccianiga, M. & Thuiller, W.
592   2021. Dynamics of Ecological Communities Following Current Retreat of Glaciers. *Annual Review of Ecology, Evolution, and*
593   *Systematics,* 52**,** 405-426.

594   Fickert, T. & Grüninger, F. 2018. High-speed colonization of bare ground-Permanent plot studies on primary succession of plants in recently
595   deglaciated glacier forelands. *Land Degradation & Development,* 29**,** 2668-2680.

596   Fischer, A., Fickert, T., Schwaizer, G., Patzelt, G. & Gross, G. 2019. Vegetation dynamics in Alpine glacier forelands tackled from space.
597   *Scientific Reports,* 9**,** 13918.

598   Franzén, M., Dieker, P., Schrader, J. & Helm, A. 2019. Rapid plant colonization of the forelands of a vanishing glacier is strongly associated
599   with species traits. *Arctic, Antarctic, and Alpine Research,* 51**,** 366-378.

600   Fretwell, P. T., Convey, P., Fleming, A. H., Peat, H. J. & Hughes, K. A. 2011. Detecting and mapping vegetation distribution on the Antarctic
601   Peninsula from remote sensing data. *Polar Biology,* 34**,** 273-281.

602   Garbarino, M., Lingua, E., Nagel, T. A., Godone, D., Motta, R. 2010. Patterns of larch establishment following deglaciation of Ventina
603   glacier, central Italian Alps. Forest Ecology and Management, 259 (3), 583-590.

604   Gardent, M., Rabatel, A., Dedieu, J.-P. & Deline, P. 2014. Multitemporal glacier inventory of the French Alps from the late 1960s to the late
605   2000s. *Global and Planetary Change,* 120**,** 24-37.

606   Garibotti, I. A., Pissolito, C. I. & Villalba, R. 2011. Spatiotemporal Pattern of Primary Succession in Relation to Meso-topographic Gradients
607   on Recently Deglaciated Terrains in the Patagonian Andes. *Arctic, Antarctic, and Alpine Research,* 43**,** 555-567.

608   Gascoin, S., Grizonnet, M., Bouchet, M., Salgues, G. & Hagolle, O. 2019. Theia Snow collection: high-resolution operational snow cover
609   maps from Sentinel-2 and Landsat-8 data. *Earth System Science Data,* 11**,** 493-514.

610   Gobiet, A., Kotlarski, S., Beniston, M., Heinrich, G., Rajczak, J. & Stoffel, M. 2014. 21st century climate change in the European Alps--a
611   review. *Science of the Total Environment,* 493**,** 1138-51.

612   Górniak, D., Marszałek, H., Kwaśniak-Kominek, M., Rzepa, G. & Manecki, M. 2017. Soil formation and initial microbiological activity on
613   a foreland of an Arctic glacier (SW Svalbard). *Applied Soil Ecology,* 114**,** 34-44.

614   Greenwell, B. M. 2017. pdp: An R Package for Constructing Partial Dependence Plots. *The R Journal,* 9**,** 421.

615   Gurnell, A. M., Edwards, P. J., Petts, G. E. & Ward, J. V. 2000. A conceptual model for alpine proglacial river channel evolution under
616   changing climatic conditions. *Catena,* 38**,** 223-242.

617   Gurnell, A. M., Petts, G. E., Hannah, D. M., Smith, B. P. G., Edwards, P. J., Kollmann, J., Ward, J. V. & Tockner, K. 2001. Riparian
618   vegetation and island formation along the gravel-bed Fiume Tagliamento, Italy. *Earth Surface Processes and Landforms,* 26**,** 31-
619   62.

620   Haeberli, W., Schaub, Y. & Huggel, C. 2017. Increasing risks related to landslides from degrading permafrost into new lakes in de-glaciating
621   mountain ranges. *Geomorphology,* 293**,** 405-417.

622   Healy, S. M., Khan, A. L. 2022. Mapping glacier ablation with a UAV in the North Cascades: A structure-from-motion approach. Frontiers
623   in Remote Sensing, 57.

16

Heckmann, T., Mccoll, S. & Morche, D. 2016. Retreating ice: research in pro-glacial areas matters. *Earth Surface Processes and Landforms,* 41**,** 271-276.

Huss, M., Bookhagen, B., Huggel, C., Jacobsen, D., Bradley, R. S., Clague, J. J., Vuille, M., Buytaert, W., Cayan, D. R., Greenwood, G., Mark, B. G., Milner, A. M., Weingartner, R. & Winder, M. 2017. Toward mountains without permanent snow and ice. *Earth's Future,* 5**,** 418-435.

Hutchinson, M. F., Xu, T. & Stein, J. A. 2011. Recent progress in the ANUDEM elevation gridding procedure. *Geomorphometry*.

Johnson, E. A. & Miyanishi, K. 2008. Testing the assumptions of chronosequences in succession. *Ecology Letters,* 11**,** 419-31.

Joly, D. & Brossard, T. 2007. Contribution of environmental factors to temperature distribution at different resolution levels on the forefield of the Loven Glaciers, Svalbard. *Polar Record,* 43**,** 353-359.

Khedim, N., Cecillon, L., Poulenard, J., Barre, P., Baudin, F., Marta, S., Rabatel, A., Dentant, C., Cauvy-Fraunie, S., Anthelme, F., Gielly, L., Ambrosini, R., Franzetti, A., Azzoni, R. S., Caccianiga, M. S., Compostella, C., Clague, J., Tielidze, L., Messager, E., Choler, P. & Ficetola, G. F. 2021. Topsoil organic matter build-up in glacier forelands around the world. *Global Change Biology,* 27**,** 1662-1677.

Klaar, M. J., Kidd, C., Malone, E., Bartlett, R., Pinay, G., Chapin, F. S. & Milner, A. 2015. Vegetation succession in deglaciated landscapes: implications for sediment and landscape stability. *Earth Surface Processes and Landforms,* 40**,** 1088-1100.

Knoflach, B., Ramskogler, K., Talluto, M., Hofmeister, F., Haas, F., Heckmann, T., Pfeiffer, M., Piermattei, L., Ressl, C., Wimmer, M. H., Geitner, C., Erschbamer, B. & Stötter, J. 2021. Modelling of Vegetation Dynamics from Satellite Time Series to Determine Proglacial Primary Succession in the Course of Global Warming—A Case Study in the Upper Martell Valley (Eastern Italian Alps). *Remote Sensing,* 13**,** 4450.

Lane, S. N., Borgeaud, L. & Vittoz, P. 2016. Emergent geomorphic-vegetation interactions on a subalpine alluvial fan. *Earth Surface Processes and Landforms,* 41**,** 72-86.

Lang, N., Irniger, A., Rozniak, A., Hunziker, R., Wegner, J. D. & Schindler, K. 2021. GRAINet: mapping grain size distributions in river beds from UAV images with convolutional neural networks. *Hydrology and Earth System Sciences,* 25**,** 2567-2597.

Langhammer, L., Grab, M., Bauder, A. & Maurer, H. 2019. Glacier thickness estimations of alpine glaciers using data and modeling constraints. *The Cryosphere,* 13**,** 2189-2202.

Lardeux, P., Glasser, N., Holt, T. & Hubbard, B. 2015. Glaciological and geomorphological map of Glacier Noir and Glacier Blanc, French Alps. *Journal of Maps,* 12**,** 582-596.

Legendre, P. & Gallagher, E. D. 2001. Ecologically meaningful transformations for ordination of species data. *Oecologia,* 129**,** 271-280.

Liaw, A. & Wiener, M. 2002. Classification and regression by randomForest. *R News,* 2/3.

Linsbauer, A., Huss, M., Hodel, E., Bauder, A., Fischer, M., Weidmann, Y., Bärtschi, H. & Schmassmann, E. 2021. The New Swiss Glacier Inventory SGI2016: From a Topographical to a Glaciological Dataset. *Frontiers in Earth Science,* 9.

Mainetti, A., D'amico, M., Probo, M., Quaglia, E., Ravetto Enri, S., Celi, L. & Lonati, M. 2021. Successional Herbaceous Species Affect Soil Processes in a High-Elevation Alpine Proglacial Chronosequence. *Frontiers in Environmental Science,* 8.

Markham, B. L. & Helder, D. L. 2012. Forty-year calibrated record of earth-reflected radiance from Landsat: A review. *Remote Sensing of Environment,* 122**,** 30-40.

Marta, S., Azzoni, R. S., Fugazza, D., Tielidze, L., Chand, P., Sieron, K., Almond, P., Ambrosini, R., Anthelme, F., Alviz Gazitúa, P., Bhambri, R., Bonin, A., Caccianiga, M., Cauvy-Fraunié, S., Ceballos Lievano, J. L., Clague, J., Cochachín Rapre, J. A., Dangles, O., Deline, P., Eger, A., Cruz Encarnación, R., Erokhin, S., Franzetti, A., Gielly, L., Gili, F., Gobbi, M., Guerrieri, A., Hågvar, S., Khedim, N., Kinyanjui, R., Messager, E., Morales-Martínez, M. A., Peyre, G., Pittino, F., Poulenard, J., Seppi, R., Chand Sharma, M., Urseitova, N., Weissling, B., Yang, Y., Zaginaev, V., Zimmer, A., Diolaiuti, G. A., Rabatel, A. & Ficetola, G. F. 2021. The Retreat of Mountain Glaciers since the Little Ice Age: A Spatially Explicit Database. *Data,* 6**,** 107.

Marteinsdóttir, B., Svavarsdóttir, K. & Thórhallsdóttir, T. E. 2010. Development of vegetation patterns in early primary succession. *Journal of Vegetation Science,* 21**,** 531-540.

Martín-Ortega, P., García-Montero, L. G. & Sibelet, N. 2020. Temporal Patterns in Illumination Conditions and Its Effect on Vegetation Indices Using Landsat on Google Earth Engine. *Remote Sensing,* 12**,** 211.

Masek, J. G., Vermote, E. F., Saleous, N. E., Wolfe, R., Hall, F. G., Huemmrich, K. F., Gao, F., Kutler, J. & Lim, T. K. 2006. A Landsat Surface Reflectance Dataset for North America, 1990–2000. *IEEE Geoscience and Remote Sensing Letters,* 3**,** 68-72.

Matthews, J. A. & Briffa, K. R. 2005. The 'little ice age': re-evaluation of an evolving concept. *Geografiska Annaler: Series A, Physical Geography,* 87**,** 17-36.

Miller, H. R. & Lane, S. N. 2018. Biogeomorphic feedbacks and the ecosystem engineering of recently deglaciated terrain. *Progress in Physical Geography: Earth and Environment,* 43**,** 24-45.

Minchin, P. R. 1987. An evaluation of the relative robustness of techniques for ecological ordination. *Vegetatio,* 69**,** 89-107.

Mong, C. E. & Vetaas, O. R. 2006. Establishment of Pinus Wallichiana on a Himalayan Glacier Foreland: Stochastic Distribution or Safe Sites? *Arctic, Antarctic, and Alpine Research,* 38**,** 584-592.

Moreau, M., Mercier, D., Laffly, D. & Roussel, E. 2008. Impacts of recent paraglacial dynamics on plant colonization: A case study on Midtre Lovénbreen foreland, Spitsbergen (79°N). *Geomorphology,* 95**,** 48-60.

17

680 Nagol, J. R., Sexton, J. O., Kim, D.-H., Anand, A., Morton, D., Vermote, E. & Townshend, J. R. 2015. Bidirectional effects in Landsat
681   reflectance estimates: Is there a problem to solve? *ISPRS Journal of Photogrammetry and Remote Sensing,* 103**,** 129-135.
682 Oksanen, J., Blanchet, F. G., Friendly, M., Kindt, R., Legendre, P., Mcglinn, D., Minchin, P. R., O'hara, R. B., Simpson, G. L., Solymos, P.,
683   Henry, M., H. Stevens, Szoecs, E. & Wagner, H. 2020. vegan: Community Ecology Package.
684 Ormsby, J. P., Choudhury, B. J. & Owe, M. 1987. Vegetation spatial variability and its effect on vegetation indices. *International Journal*
685   *of Remote Sensing,* 8**,** 1301-1306.
686 Painter, T. H., Flanner, M. G., Kaser, G., Marzeion, B., Vancuren, R. A. & Abdalati, W. 2013. End of the Little Ice Age in the Alps forced
687   by industrial black carbon. *Proceedings of the National Academy of Sciences of the United States of America,* 110, 15216-21.
688 Pickett, S. T. A. 1989. Space-for-Time Substitution as an Alternative to Long-Term Studies. 110-135.
689 Pinheiro, J., Bates, D., R Core Team 2022. Nlme: Linear and Nonlinear Mixed Effects Models R package version 3.1-160 https://CRAN.R-
690   project.org/package=nlme
691 Qiu, S., He, B., Zhu, Z., Liao, Z. & Quan, X. 2017. Improving Fmask cloud and cloud shadow detection in mountainous area for Landsats
692   4–8 images. *Remote Sensing of Environment,* 199**,** 107-119.
693 Qiu, S., Lin, Y., Shang, R., Zhang, J., Ma, L. & Zhu, Z. 2019a. Making Landsat Time Series Consistent: Evaluating and Improving Landsat
694   Analysis Ready Data. *Remote Sensing,* 11**,** 51.
695 Qiu, S., Zhu, Z. & He, B. 2019b. Fmask 4.0: Improved cloud and cloud shadow detection in Landsats 4–8 and Sentinel-2 imagery. *Remote*
696   *Sensing of Environment,* 231**,** 111205.
697 Raffl, C., Mallaun, M., Mayer, R. & Erschbamer, B. 2006. Vegetation Succession Pattern and Diversity Changes in a Glacier Valley, Central
698   Alps, Austria. *Arctic, Antarctic, and Alpine Research,* 38**,** 421-428.
699 Robbins, J. A. & Matthews, J. A. 2010. Regional Variation in Successional Trajectories and Rates of Vegetation Change on Glacier Forelands
700   in South-Central Norway. *Arctic, Antarctic, and Alpine Research,* 42**,** 351-361.
701 Robbins, J. A. & Matthews, J. A. 2014. Use of ecological indicator values to investigate successional change in boreal to high-alpine glacier-
702   foreland chronosequences, southern Norway. *The Holocene,* 24**,** 1453-1464.
703 Rosero, P., Crespo-Pérez, V., Espinosa, R., Andino, P., Barragán, Á., Moret, P., Gobbi, M., Ficetola, G. F., Jaramillo, R., Muriel, P.,
704   Anthelme, F., Jacobsen, D., Dangles, O., Condom, T., Gielly, L., Poulenard, J., Rabatel, A., Basantes, R., Cáceres Correa, B. &
705   Cauvy-Frauníe, S. 2021. Multi-taxa colonisation along the foreland of a vanishing equatorial glacier. *Ecography,* 44**,** 1010-1021.
706 Roy, D. P., Kovalskyy, V., Zhang, H. K., Vermote, E. F., Yan, L., Kumar, S. S. & Egorov, A. 2016a. Characterization of Landsat-7 to
707   Landsat-8 reflective wavelength and normalized difference vegetation index continuity. *Remote Sensing of Environment,* 185**,** 57-
708   70.
709 Roy, D. P., Zhang, H. K., Ju, J., Gomez-Dans, J. L., Lewis, P. E., Schaaf, C. B., Sun, Q., Li, J., Huang, H. & Kovalskyy, V. 2016b. A general
710   method to normalize Landsat reflectance data to nadir BRDF adjusted reflectance. *Remote Sensing of Environment,* 176**,** 255-271.
711 Rydgren, K., Halvorsen, R., Töpper, J. P., Njøs, J. M. & Del Moral, R. 2014. Glacier foreland succession and the fading effect of terrain
712   age. *Journal of Vegetation Science,* 25**,** 1367-1380.
713 Schaaf, C. B., Gao, F., Strahler, A. H., Lucht, W., Li, X., Tsang, T., Strugnell, N. C., Zhang, X., Jin, Y., Muller, J.-P., Lewis, P., Barnsley,
714   M., Hobson, P., Disney, M., Roberts, G., Dunderdale, M., Doll, C., D'entremont, R. P., Hu, B., Liang, S., Privette, J. L. & Roy, D.
715   2002. First operational BRDF, albedo nadir reflectance products from MODIS. *Remote Sensing of Environment,* 83**,** 135-148.
716 Scherrer, D. & Körner, C. 2011. Topographically controlled thermal-habitat differentiation buffers alpine plant diversity against climate
717   warming. *Journal of Biogeography,* 38**,** 406-416.
718 Schumann, K., Gewolf, S. & Tackenberg, O. 2016. Factors affecting primary succession of glacier foreland vegetation in the European Alps.
719   *Alpine Botany,* 126**,** 105-117.
720 Sigl, M., Abram, N. J., Gabrieli, J., Jenk, T. M., Osmont, D. & Schwikowski, M. 2018. 19th century glacier retreat in the Alps preceded the
721   emergence of industrial black carbon deposition on high-alpine glaciers. *The Cryosphere,* 12**,** 3311-3331.
722 Soenen, S. A., Peddle, D. R. & Coburn, C. A. 2005. SCS+C: a modified Sun-canopy-sensor topographic correction in forested terrain. *IEEE*
723   *Transactions on Geoscience and Remote Sensing,* 43**,** 2148-2159.
724 Sola, I., González-Audícana, M. & Álvarez-Mozos, J. 2016. Multi-criteria evaluation of topographic correction methods. *Remote Sensing of*
725   *Environment,* 184**,** 247-262.
726 Steven, M. D., Malthus, T. J., Baret, F., Xu, H. & Chopping, M. J. 2003. Intercalibration of vegetation indices from different sensor systems.
727   *Remote Sensing of Environment,* 88**,** 412-422.
728 Stöcklin, J. & Bäumler, E. 1996. Seed rain, seedling establishment and clonal growth strategies on a glacier foreland. *Journal of Vegetation*
729   *Science,* 7**,** 45-56.
730 Tackenberg, O. & Stöcklin, J. 2008. Wind dispersal of alpine plant species: A comparison with lowland species. *Journal of Vegetation*
731   *Science,* 19**,** 109-118.
732 Temme, A. J. a. M. & Lange, K. 2014. Pro-glacial soil variability and geomorphic activity - the case of three Swiss valleys. *Earth Surface*
733   *Processes and Landforms***,** n/a-n/a.
734 Todd, S. W., Hoffer, R. M. & Milchunas, D. G. 1998. Biomass estimation on grazed and ungrazed rangelands using spectral indices.
735   *International Journal of Remote Sensing,* 19**,** 427-438.

736 Tucker, C. J. & Sellers, P. J. 1986. Satellite remote sensing of primary production. *International Journal of Remote Sensing,* 7**,** 1395-1416.
737 Vázquez-Tarrío, D., Borgniet, L., Liébault, F. & Recking, A. 2017. Using UAS optical imagery and SfM photogrammetry to characterize
738   the surface grain size of gravel bars in a braided river (Vénéon River, French Alps). *Geomorphology,* 285**,** 94-105.
739 Vernay, M., Lafaysse, M., Monteiro, D., Hagenmuller, P., Nheili, R., Samacoïts, R., Verfaillie, D. & Morin, S. 2022. The S2M
740   meteorological and snow cover reanalysis over the French mountainous areas: description and evaluation (1958–2021). *Earth*
741   *System Science Data,* 14**,** 1707-1733.
742 Vincent, C., Harter, M., Gilbert, A., Berthier, E. & Six, D. 2014. Future fluctuations of Mer de Glace, French Alps, assessed using a
743   parameterized model calibrated with past thickness changes. *Annals of Glaciology,* 55**,** 15-24.
744 Vincent, C., Le Meur, E., Six, D. & Funk, M. 2005. Solving the paradox of the end of the Little Ice Age in the Alps. *Geophysical Research*
745   *Letters,* 32.
746 Walker, L. R. & Wardle, D. A. 2014. Plant succession as an integrator of contrasting ecological time scales. *Trends in Ecology & Evolution,*
747   29**,** 504-10.
748 Westoby, M. J., Dunning, S. A., Woodward, J., Hein, A. S., Marrero, S. M., Winter, K. & Sugden, D. E. 2017. Sedimentological
749   characterization of Antarctic moraines using UAVs and Structure-from-Motion photogrammetry. *Journal of Glaciology,* 61**,** 1088-
750   1102.
751 Wittich, K.-P. & Hansing, O. 1995. Area-averaged vegetative cover fraction estimated from satellite data. *International Journal of*
752   *Biometeorology,* 38**,** 209-215.
753 Wojcik, R., Donhauser, J., Frey, B. & Benning, L. G. 2020. Time since deglaciation and geomorphological disturbances determine the
754   patterns of geochemical, mineralogical and microbial successions in an Icelandic foreland. *Geoderma,* 379**,** 114578.
755 Wojcik, R., Eichel, J., Bradley, J. A. & Benning, L. G. 2021. How allogenic factors affect succession in glacier forefields. *Earth-Science*
756   *Reviews,* 218**,** 103642.
757 Woellner, R., Wagner, T. C. 2019. Saving species, time and money: Application of unmanned aerial vehicles (UAVs) for monitoring of an
758   endangered alpine river specialist in a small nature reserve. Biological conservation, 233, 162-175.
759 Wulder, M. A., Loveland, T. R., Roy, D. P., Crawford, C. J., Masek, J. G., Woodcock, C. E., Allen, R. G., Anderson, M. C., Belward, A. S.,
760   Cohen, W. B., Dwyer, J., Erb, A., Gao, F., Griffiths, P., Helder, D., Hermosilla, T., Hipple, J. D., Hostert, P., Hughes, M. J.,
761   Huntington, J., Johnson, D. M., Kennedy, R., Kilic, A., Li, Z., Lymburner, L., Mccorkel, J., Pahlevan, N., Scambos, T. A., Schaaf,
762   C., Schott, J. R., Sheng, Y., Storey, J., Vermote, E., Vogelmann, J., White, J. C., Wynne, R. H. & Zhu, Z. 2019. Current status of
763   Landsat program, science, and applications. *Remote Sensing of Environment,* 225**,** 127-147.
764 Zhang, H. K., Roy, D. P. & Kovalskyy, V. 2016. Optimal Solar Geometry Definition for Global Long-Term Landsat Time-Series
765   Bidirectional Reflectance Normalization. *IEEE Transactions on Geoscience and Remote Sensing,* 54**,** 1410-1418.
766 Zhu, Z. & Woodcock, C. E. 2012. Object-based cloud and cloud shadow detection in Landsat imagery. *Remote Sensing of Environment,*
767   118**,** 83-94.
768 Zhu, Z. & Woodcock, C. E. 2014. Automated cloud, cloud shadow, and snow detection in multitemporal Landsat data: An algorithm designed
769   specifically for monitoring land cover change. *Remote Sensing of Environment,* 152**,** 217-234.
770 Zimmer, A., Meneses, R. I., Rabatel, A., Soruco, A., Dangles, O. & Anthelme, F. 2018. Time lag between glacial retreat and upward
771   migration alters tropical alpine communities. *Perspectives in Plant Ecology, Evolution and Systematics,* 30**,** 89-102.

772

773

774

775

776

777

778

779

780

781

782

783

784

785
786
787
788
789
790
791
792
793
794
795
796
797
798
799
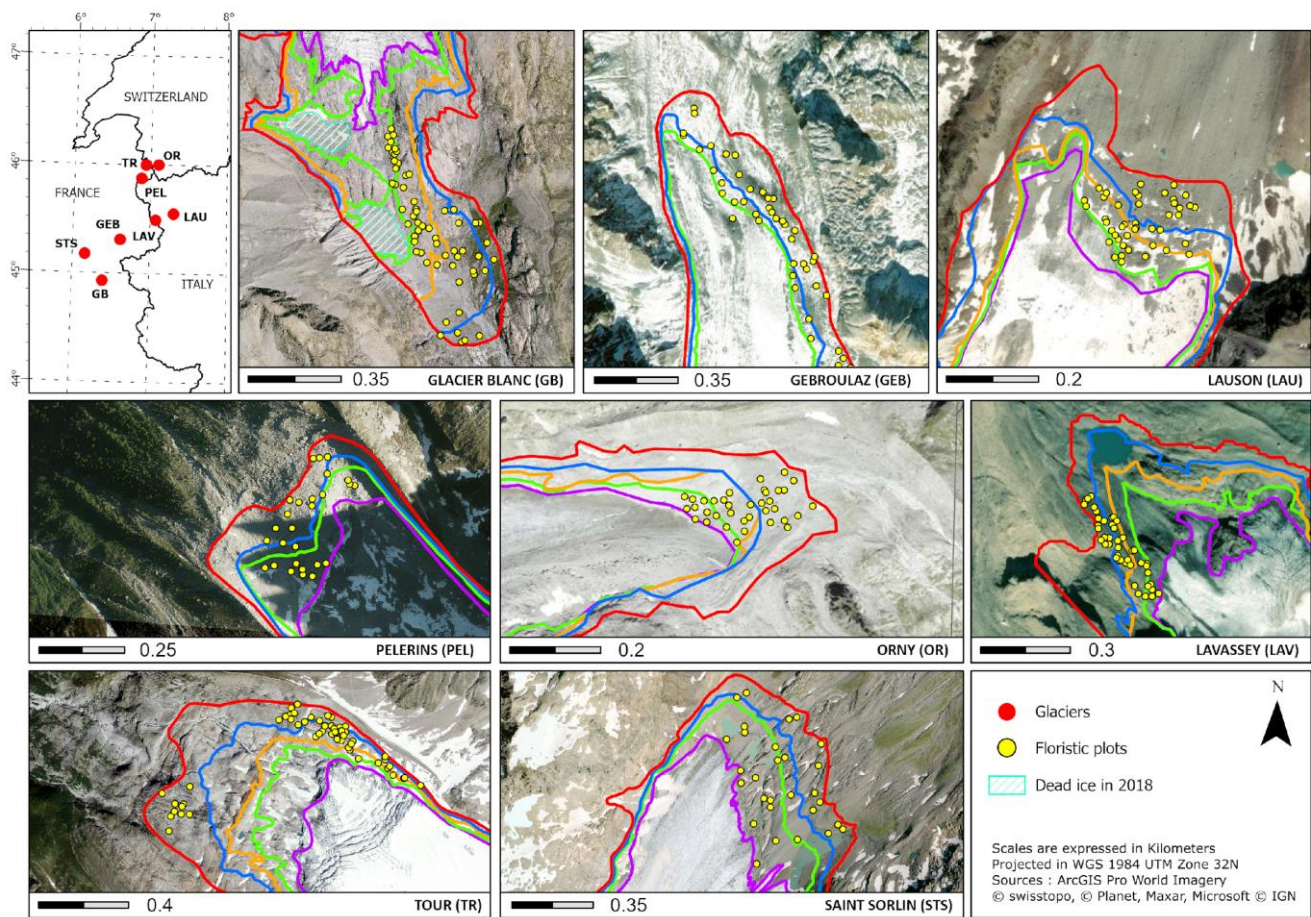
Figure 1. Distribution of the eight   glacier margins in France, Switzerland, and Italy with corresponding abbreviations. Floristic plots are indicated in yellow points while glacier outlines are shown in thick coloured lines. Colours do not indicate similar outlines date but chronosequence of deglaciation. Corresponding years of deglaciation is to be found in Table S1. Projection and sources details are indicated in the bottom right panel.
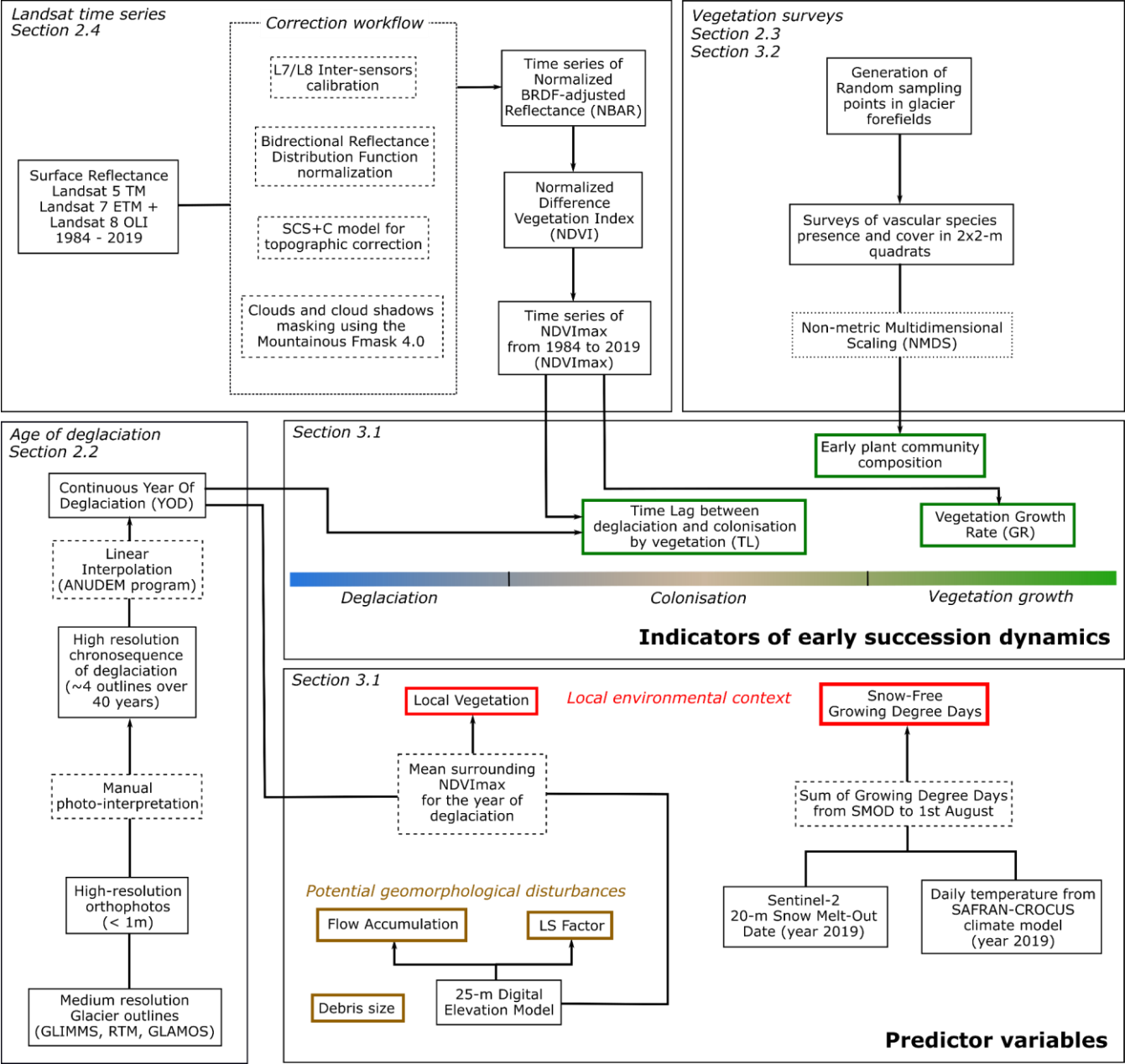
Figure 2. Complete analysis workflow shown by methodological sections. Indicators of early succession dynamics are shown in green while predictor variables are shown in red and brown.
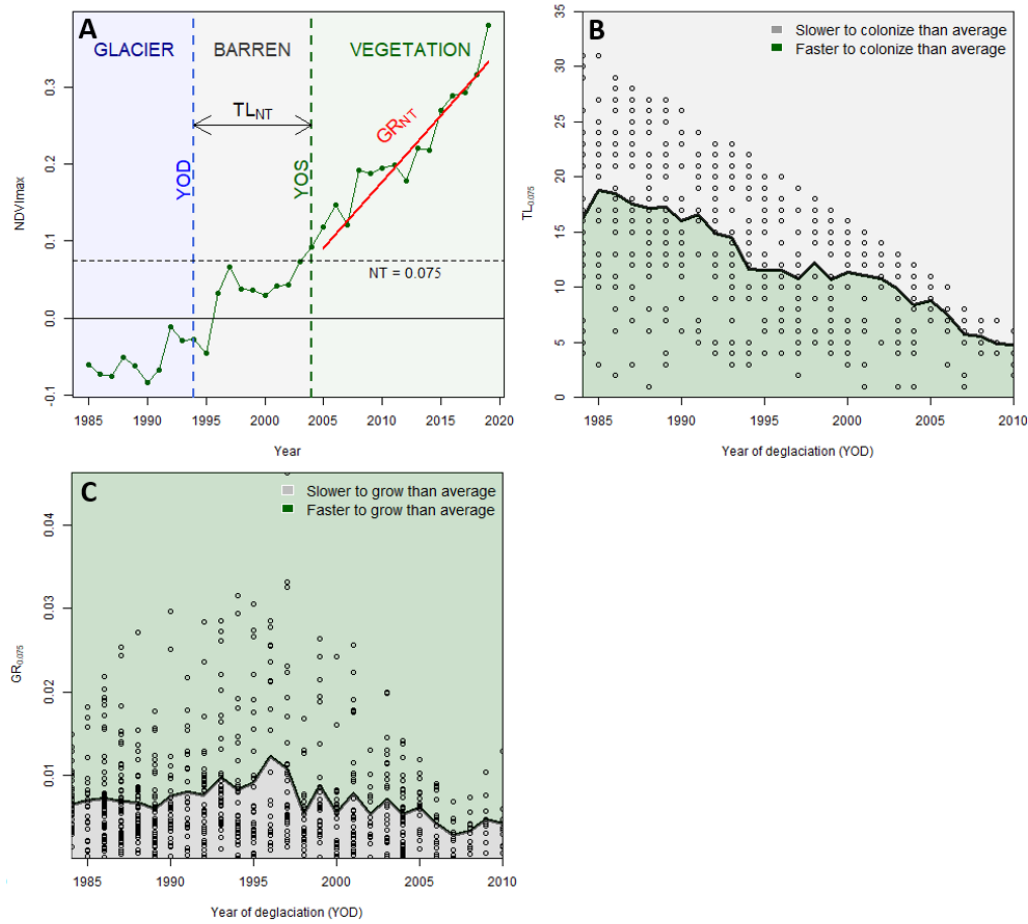
Figure 3. (A) Example of indicators derived from the Landsat-based NDVImax time series and deglaciation data for a single pixel located in the Glacier Blanc forefield (latitude: 44.932938 and longitude: 6.409681). (B) Time Lag (TL) and (C) Growth Rate (GR) for an NDVI threshold of 0.75　　for the eight　　margins according to year of deglaciation. Thick black lines represent the median value for each year of deglaciation used to compute anomalies. Green shaded areas represent faster colonization and growth rate than average, while slower than average growth rates are indicated by grey shaded areas.
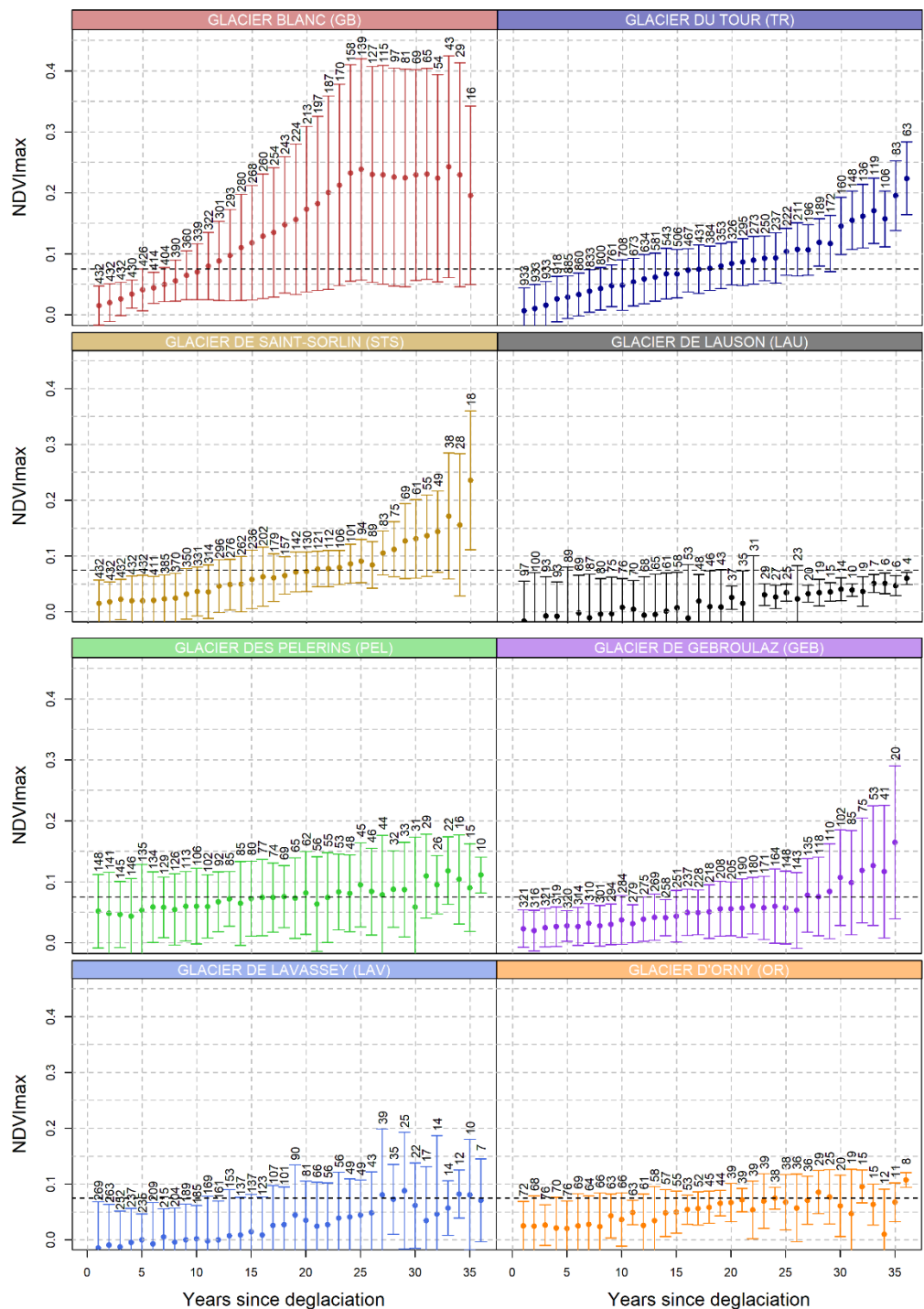
821   **Figure 4.** Distribution of NDVImax values according to the number of years since deglaciation for the eight glacier forefields. Error bars
822   indicate standard deviation and numbers indicate the numbers of pixels for a given number of years since deglaciation. Horizontal dashed
823   lines show an NDVI of 0.075. Numbers of pixels for each year since deglaciation are indicated above each error bar.
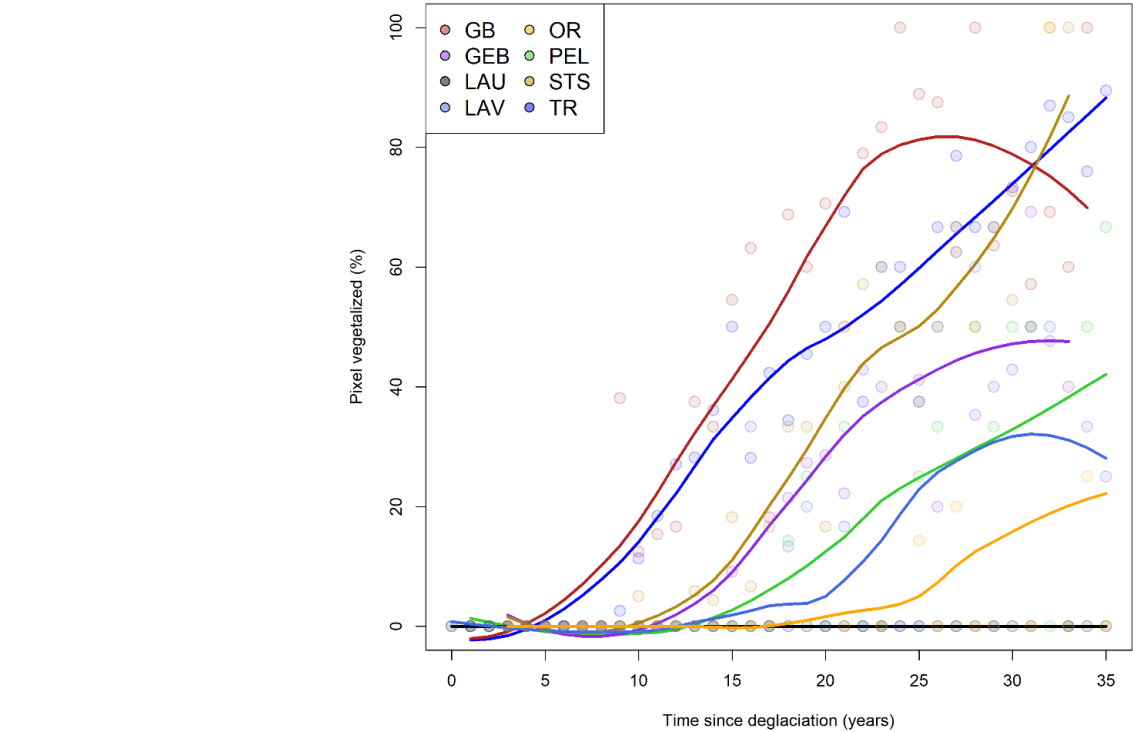

824
825   **Figure 5**. Proportion of pixels identified as vegetated according to time since deglaciation for all pixels within the eight glacier forefields.
826   Trend   lines are computed from loess function with span = 0.7.
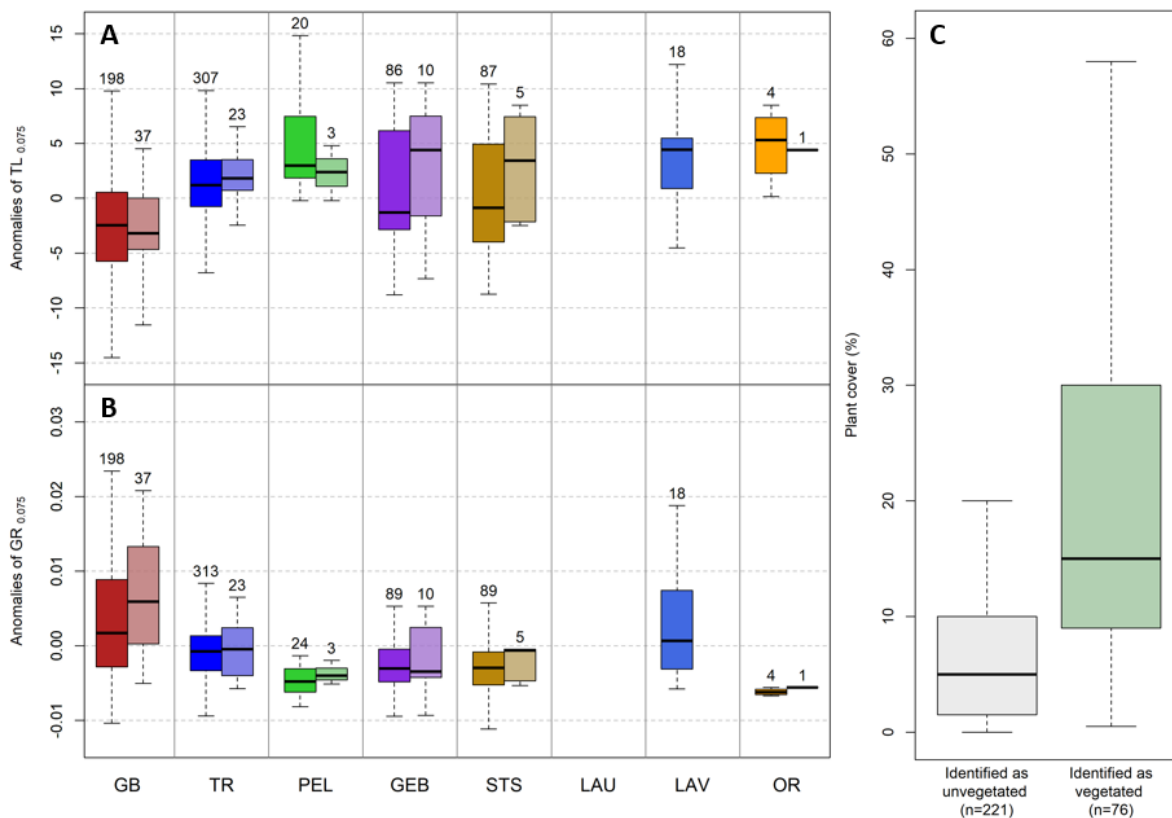
Figure 6. Distribution of (A) Time Lag and (B) Growth Rate anomalies for the eight glacier margins for an NDVI threshold of 0.075. For each glacier, the left boxplot with full colours corresponds to all pixels while the right boxplot with shaded colours corresponds only to pixel overlapping floristic plots. (C) Distribution of plant cover (%) for floristic plots that have been identified as vegetated/unvegetated based on the remote sensing approach.
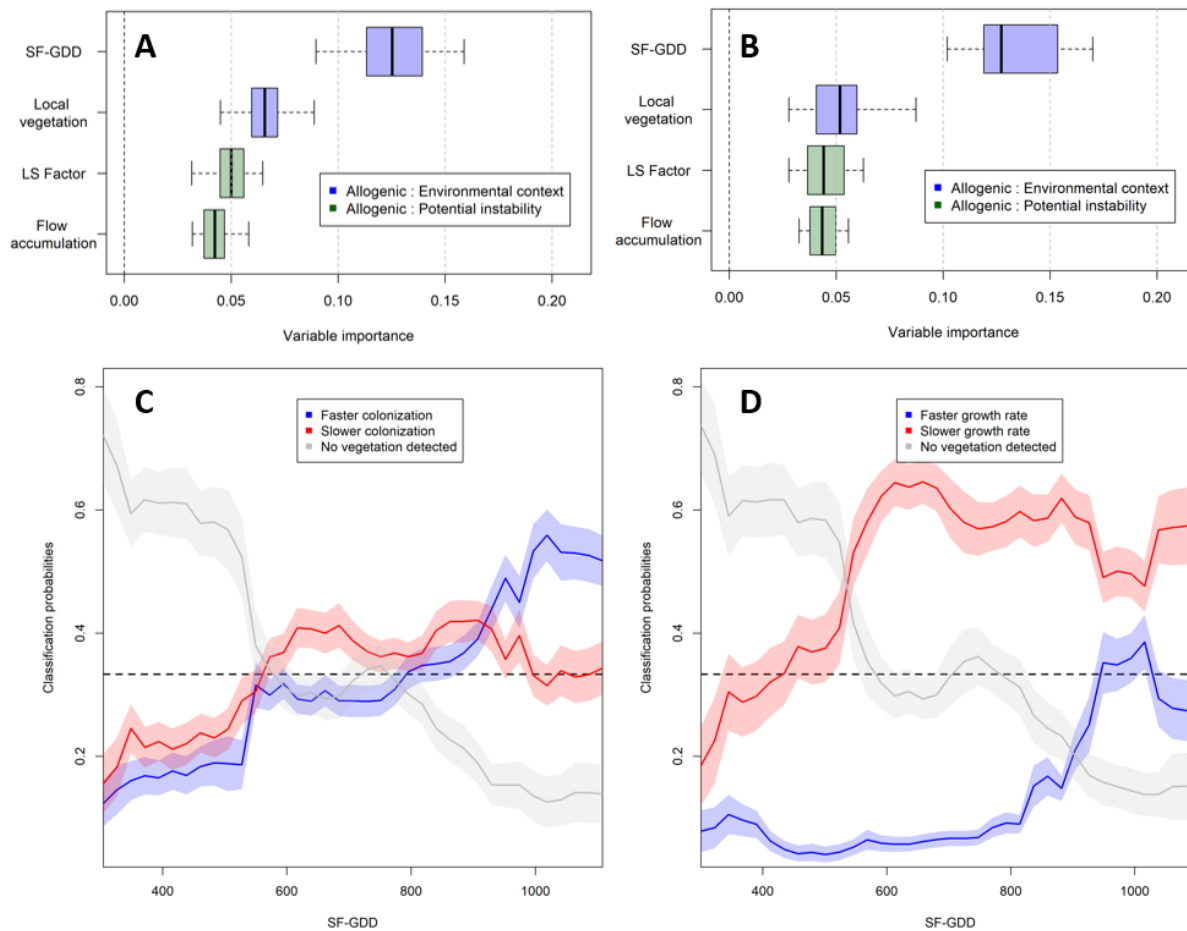
Figure 7. Variable importance from the random forest model considering the three classes of (A) TL and (B) GR. Partial dependency   plots illustrating how SF-GDD affects class probability for the three classes of (C) TL and (D) GR.

27
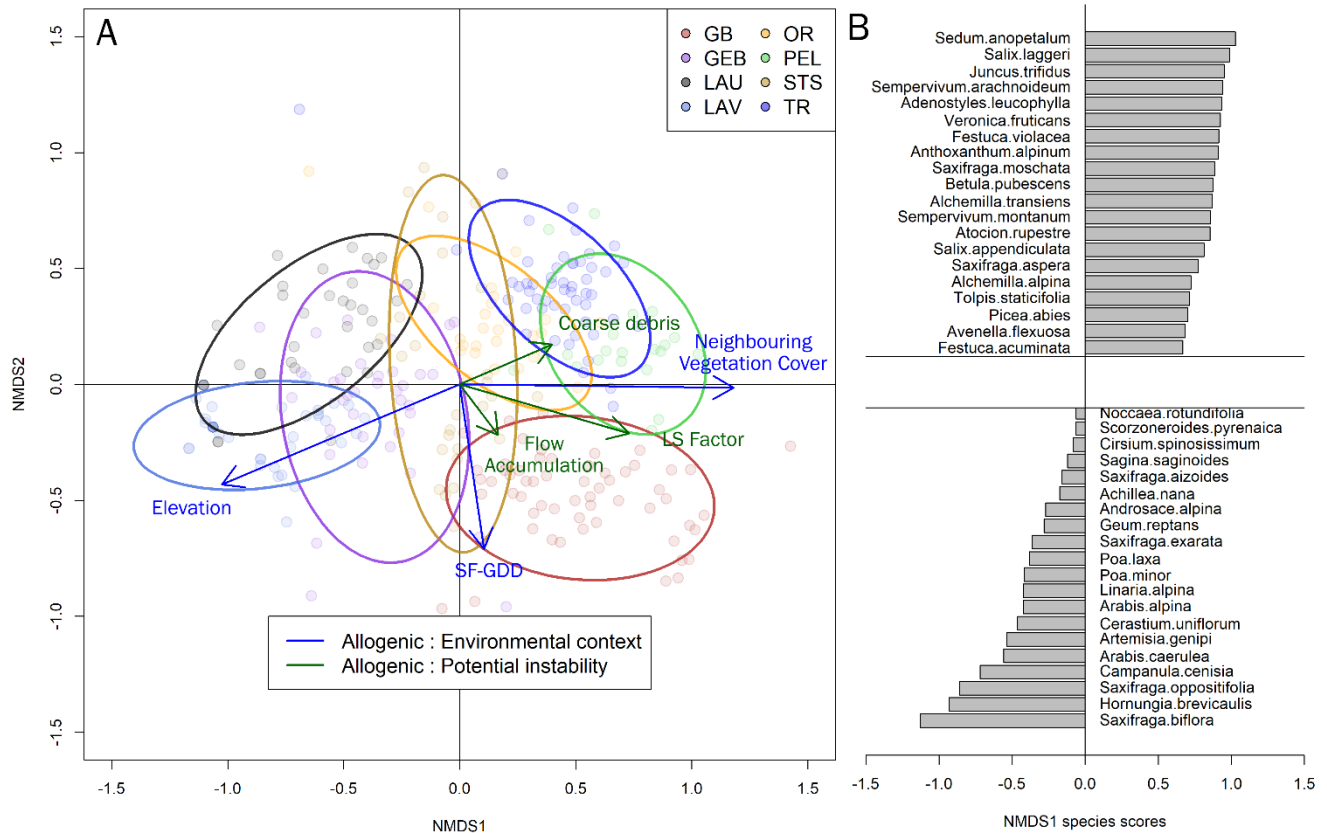
Figure 8. (A) Non-metric Multidimensional Scaling (NMDS) of floristic plots by species with vector fitting of explanatory variables implemented using Generalized Least Square (GLS) regression corrected for autocorrelated error structure. Ellipsoids correspond to an interval of 0.8 the standard deviation. The analysis includes 297 plots from the eight glacier forefields. (B) Species distribution along the NMDS axis 1 with the 20 species depicting the highest and lowest scores.
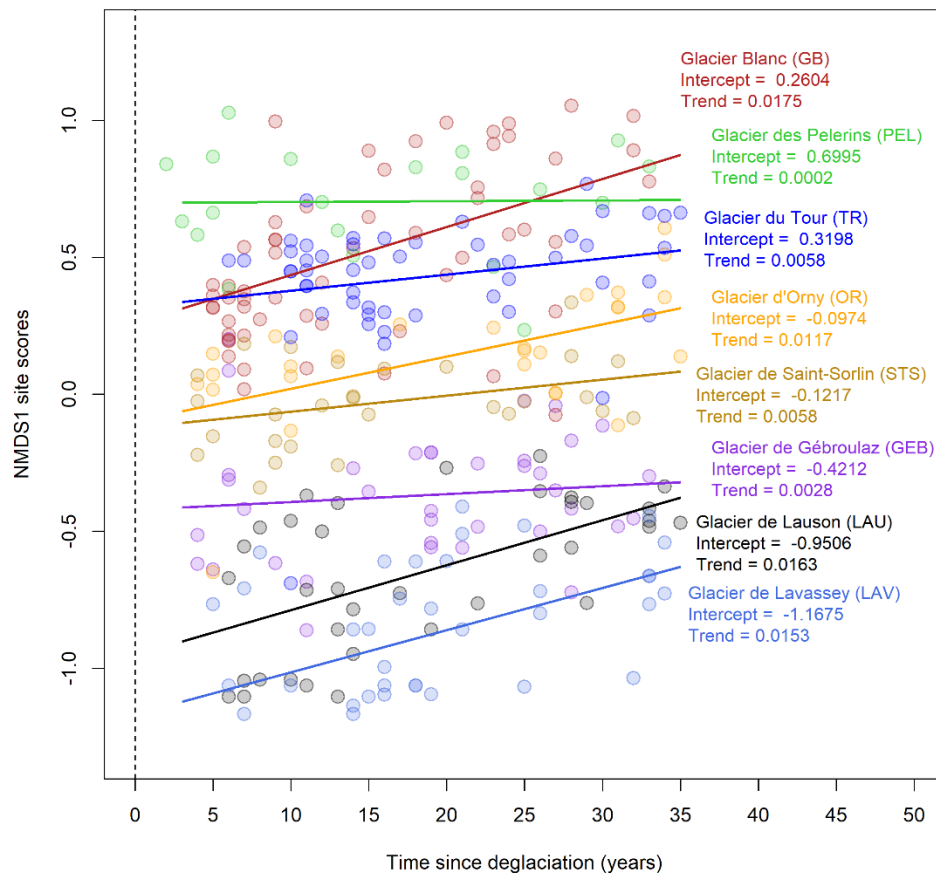
Figure 9. First axis scores of the NMDS according to time since deglaciation for the eight glacier forefields. Intercept and slope parameters are based on linear models for each glacier forefield.

847
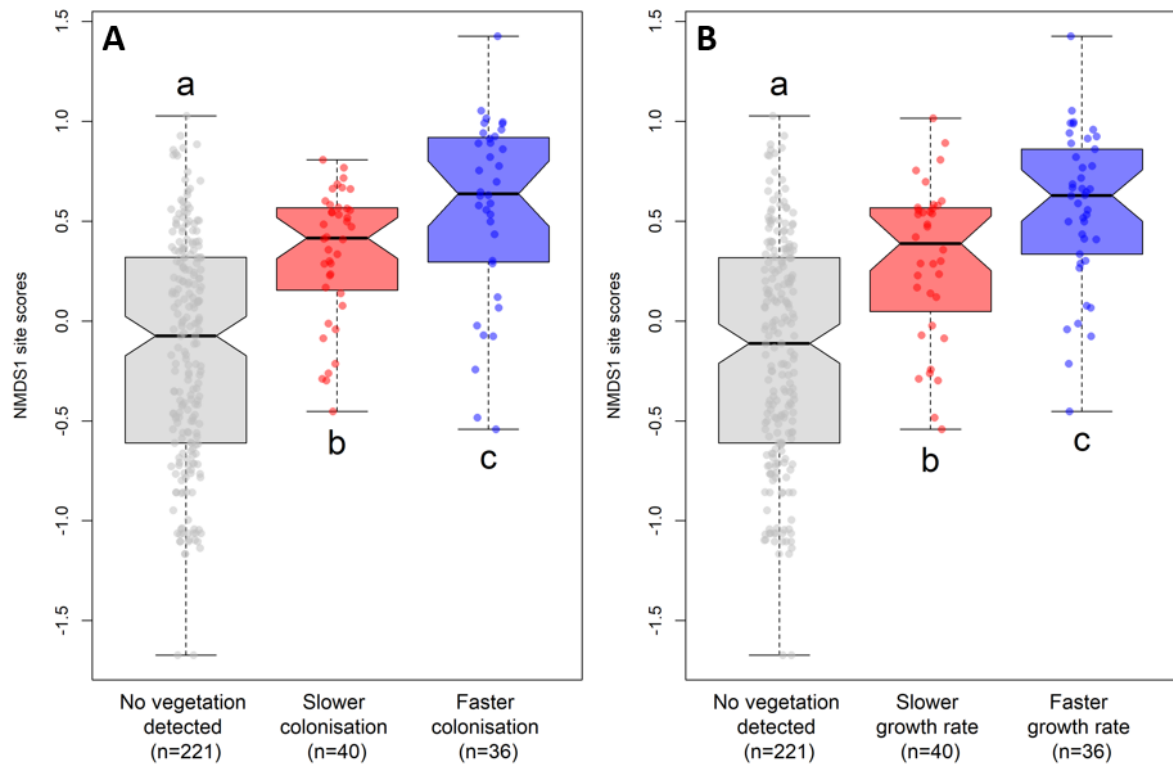
Figure 10. First axis scores of the NMDS according to the three classes of anomalies of (A) Time Lag and (B) Growth Rate for an NDVI threshold of 0.075. Letters a, b and c indicate significant differences based on the Wilcoxon test (P-values < 0.05).

850

Variables set	Variables	With autocorrelated errors structure		Corrected for autocorrelated errors structure	
		AICc	Pseudo-R²	AICc	Pseudo-R²
Environmental context	SF-GDD (°C)	464	0.738	58	0.228
	Elevation (m. a.s.l.)	528	0.674	-1074	0.550
	Neighbouring Vegetation cover (NDVI)	567	0.629	138	0.620
Potential instability	LS Factor (°)	771	0.256	775	0.256
	Coarse debris (cm)	830	0.083	834	0.083

30

Flow accumulation	846	0.040	623	0.033

851 **Table 1.** corrected Akaike Information Criterion and Pseudo-R² values for two Generalized Least Square (GLS) regression models including

852 or not the autocorrelated error structure.

853

854

855

856